An unconditionally stable fast high order method for thermal phase change models

Weiwen Wang, Mejdi Azaiez, Chuanju Xu

AN UNCONDITIONALLY STABLE FAST HIGH ORDER METHOD FOR THERMAL PHASE CHANGE MODELS*

WEIWEN WANG[1] MEJDI AZAIEZ[1,2] CHUANJU XU[1,3]

ABSTRACT. Thermal phase change problems arise in a large number of applications. In this paper, we consider a phase field model instead of the classical Stefan model to describe phenomena, which may appear in some complex phase change problems such as dendritic crystal growth, phase transformations in metallic alloys, etc. Our aim is to propose efficient and accurate schemes for the model, which is the coupling of a heat transfer equation and a phase field equation. The schemes are constructed based on an auxiliary variable approach for the phase field equation and semi-implicit treatment for the heat transfer equation. The main novelty of the paper consists in: i) construction of the efficient schemes, which only requires solving several second-order elliptic problems with constant coefficients; ii) proof of the unconditional stability of the schemes; iii) fast high order solver for the resulting equations at each time step. A series of numerical examples are presented to verify the theoretical claims and to illustrate the efficiency of our method. As far as we know, it seems this is the first attempt made for the thermal phase change model of this type.

1. INTRODUCTION

Phase change problems are widespread in mathematics, nature, science, and their applications including the phenomena of melting and solidification in materials science. One of the main difficulties in simulating phase change problems is due to the presence of moving boundary. A classical treatment of the moving boundary is the Stefan model which was named after J. Stefan, who introduced the general class of such problems in 1891[30]. The Stefan model requires to determine the temperature $U_1(x,t)$ and $U_2(x,t)$ of the solid and liquid phases. Using the the position $x = y(t)$ to represent the boundary between the phases, the problem writes

$$\lambda\rho\frac{dy}{dt} = \big(k_1\frac{\partial}{\partial x}U_1 - k_2\frac{\partial}{\partial x}U_2\big)\big|_{x=y(t)}, \tag{1.1}$$

where λ is the latent heat of crystallization per unit mass, ρ is the density of the material in its original phase state, and k_1 and k_2 are the coefficients of conductivity corresponding to the solid and liquid phases, respectively [22]. The above classical Stefan model aims to describe the free

Date: October 25, 2021.
1991 *Mathematics Subject Classification.* 65M06, 65M12, 65M70, 35R37.
Key words and phrases. Thermal phase change problem, Phase field, SAV approach, Unconditional stability, Spectral method.
*This research is partially supported by NSFC grant 11971408, NNW2018-ZT4A06 project, and NSFC/ANR joint program 51661135011/ANR-16-CE40-0026-01.
[1]School of Mathematical Sciences and Fujian Provincial Key Laboratory of Mathematical Modeling and High Performance Scientific Computing, Xiamen University, 361005 Xiamen, China. Email:wangweiwen@stu.xmu.edu.cn.
[2]Bordeaux INP, Laboratoire I2M UMR 5295, 33607 Pessac, France. Email: azaiez@u-bordeaux.fr.
[3]Corresponding author. Email: cjxu@xmu.edu.cn.

boundary problem that occurs during solid melting or liquid solidification, such as the dendritic solidification problem [4, 13, 23] and the phase transformations in metallic alloys [24].

Roughly there are two categories of methods used to solve moving boundary in thermal phase change problems, namely front tracking methods and implicit methods. Crank [7] first proposed front tracking methods using an explicit representation of the interface and proposed an elaborate collection of numerical methods. Juric & Tryggvason [13] used a fixed grid in space to calculate temperature and a moving grid on the interface to calculate interface heat sources. Later on, Segal et al. [24] suggested an adaptive grid method. The comparison results of the fixed grid and the adaptive grid is given by Murray & Landis [19], and they showed that the fixed grid method gives a more precise heat distribution in the entire domain, whereas the adaptive grid algorithm captures the interface position more accurately. Since the front tracking methods use explicit representations, it is natural that implicit methods can be applied as an improvement. Among all implicit methods, the three most commonly used are the enthalpy method, the level set method, and the phase field method. The enthalpy method proposed in [7, 18] introduces the enthalpy function which measures the total heat of the system. Lam et al. [14] extended it to solid-state phase transformations with simple conditions on the moving boundary. Also the level set method, firstly introduced in [21], has gained great popularity in solving moving boundary problems, and now it has been generalized to many problems, see, e.g., [1, 4, 20, 25, 31]. The main idea of this method is the introduction of the level set function to capture the interface position as its zero level set.

Nevertheless there are some important phenomena which can not be captured by the classical Stefan model such as dendritic crystal growth and the fusion and joining of materials. Fix [11], Collins & Levine [6], Langer [15], and Caginalp [2] introduced phase field model which was then extensively applied to phase transformation problems. In a phase field model, the phase-field variable [16] is introduced firstly, which is a continuous scalar function of time and space, usually taking values between -1 and 1 or 0 and 1. In addition, the domain can be parameterized by the phase field function which is equal to a fixed constant in each phase, smoothly but usually rapidly varies within the two phase values in the interface. The most commonly used phase field methods in the literature are based on the Kobayashi potential [32] or based on the Caginalp potential [17], and the discrepancy between them is that the free energy is defined by different methods. Fabbri & Voller [10] compared these methods in detail. Caginalp [3] performed an asymptotic analysis for the phase field methods to test whether the phase field solution converges to the sharp interface problem and to determine the parameters appearing in the model equation.

In this paper we consider a phase field method for solving thermal phase change problem. With the assumption that the material is in region Ω and $\partial\Omega$ represents its boundary, we heat or cool the material from $\partial\Omega$ at the temperature T_0. Then we introduce $u = u(\boldsymbol{x}, t) = T(\boldsymbol{x}, t) - T_m$ as the difference of absolute temperature $T(\boldsymbol{x}, t)$ and phase transition temperature T_m of the material. Here we choose the value of ϕ between -1 and 1, where -1 means the solid state and 1 means liquid. Based on the phase field approach [16], the problem can be written as

$$\begin{cases} \tau\dfrac{\partial\phi}{\partial t} = -\sigma, \\ \sigma = -\varepsilon^2\Delta\phi + F'(\phi) - \dfrac{2\rho c}{L}u, \\ \dfrac{\partial u}{\partial t} = K\Delta u - \dfrac{L}{2\rho c}\dfrac{\partial\phi}{\partial t}. \end{cases} \tag{1.2}$$

subject to Neumann or Dirichlet boundary condition or any combination of these boundary conditions. Here the parameter ε represents the sharpness of the free boundary which is proportional to the surface tension, τ is related to the relaxation time to equilibrium, ρ is the density, c is the specific heat, L is the latent heat liberated or absorbed during phase transition, K is the thermal conductivity. $F(\cdot)$ is a potential functional which is nonlinear usually. Taking the L^2 inner products of the above equation with $-\frac{\partial\phi}{\partial t}$, $\frac{\partial\phi}{\partial t}$, and $(\frac{2\rho c}{L})^2 u$ respectively, we obtain the energy dissipation law:

$$\frac{d}{dt}E(\phi,u) = -\left\|\sqrt{\tau}\frac{\partial\phi}{\partial t}\right\|^2 - K\big(\frac{2\rho c}{L}\big)^2\|\nabla u\|^2, \tag{1.3}$$

where $E(\phi,u) = \displaystyle\int_\Omega \left(\frac{\varepsilon^2}{2}|\nabla\phi|^2 + 2\big(\frac{\rho c}{L}\big)^2 u^2 + F(\phi)\right) d\boldsymbol{x}$ is the energy function, $\|\cdot\|$ stands for the standard L^2 norm.

Therefore, the model can be considered as a heat equation coupled with a Allen-Cahn equation. The first two equations in (1.2) are expressed in the form of gradient flows. There are several popular numerical approaches to construct stable schemes for gradient flows. Among them, the first approach is the convex splitting method which appears to be introduced in [8] and popularized by [9]. The main idea is to split the free energy density $F(\phi)$ into two convex functionals, namely, $F(\phi) = F_c(\phi) - F_e(\phi)$ with $F_c''(\phi), F_e''(\phi) \geq 0$. Then the first order scheme can be constructed with the nonlinear term $F'(\phi)$ approximated by $F_c'(\phi^{n+1}) - F_e'(\phi^n)$. It is unconditionally energy stable and uniquely solvable, and at each time step it will lead to a convex minimization problem. It is believed there is no general functional splitting to construct unconditionally stable higher order schemes. In addition to the convex splitting method, stabilized linearly implicit approach [29, 40] was also widely used. In order to balance the explicit treatment of the nonlinear term, the key is to introduce an artificial stabilization term. The main advantage of the stabilized scheme is its effectiveness and simplicity, particularly when fast Poisson solvers are available [35]. However, it will result in additional accuracy issues and may not be easy to construct unconditionally stable schemes of second order. Later on, the invariant energy quadratization (IEQ), was proposed in a number of papers [33, 34, 38, 39]. It is a generalization of the method of Lagrange multipliers or of auxiliary variable. The IEQ approach has proven to be a powerful framework to construct second order unconditionally stable schemes. It is applicable to a large class of gradient flows and some dendritic crystal growth models [36, 37]. Recently the so-called scalar auxiliary variable (SAV) approach was introduced in [27], which takes the advantage of the IEQ approach while overcomes some of its drawbacks [28]. The SAV approach has been found to be a quite general tool to construct efficient schemes with fewer restrictions on the energy functionals for various equations [5, 12].

The goal of this paper is to design efficient methods for numerical solutions of the thermal phase field model. The proposed methods are based on an auxiliary variable approach for the

time discretization and spectral method for the spatial discretization. Our main contributions in this paper are threefold: (i) An unconditionally stable method for the time discretization of the heat and Allen-Cahn coupled equation modeling the thermal phase change, which to our knowledge is the first of its kind. (ii) A fast spectral method for the spatial discretization, together with the detailed implementation technique. (iii) Stability analysis of the proposed method and numerical validation of its efficiency.

The paper is organized as follows: In Section 2, we propose some first and second order schemes based on an auxiliary variable approach for the thermal phase field model, and prove the unconditional stability for the proposed schemes. In Section 3, we present the full discretization using the spectral method for the spatial approximation and describe the fast solver. Numerical experiments are given in Section 4 to validate the proposed schemes. Finally, the paper ends with some concluding remarks in Section 5.

2. Construction of the schemes and stability analysis

Throughout this paper, we assume $E_1(\phi) := \int_\Omega F(\phi)d\boldsymbol{x}$ is bounded from below, i.e., there always exists a non-negative constant C_0 such that $E_1(\phi)+C_0 > 0$. This assumption is generally true for the free energy of many physically interesting models. We now introduce the scalar auxiliary variable as follows:

$$r(t) = \sqrt{E_1(\phi)+C_0},$$

Then the model (1.2) can be rewritten as:

$$\begin{cases} \tau\dfrac{\partial\phi}{\partial t} = -\sigma, \\ \sigma = -\varepsilon^2\Delta\phi + \dfrac{r(t)}{\sqrt{E_1(\phi)+C_0}}F'(\phi) - \dfrac{2\rho c}{L}u, \\ \dfrac{dr}{dt} = \dfrac{1}{2\sqrt{E_1(\phi)+C_0}}\displaystyle\int_\Omega F'(\phi)\frac{\partial\phi}{\partial t}d\boldsymbol{x}, \\ \dfrac{\partial u}{\partial t} = K\Delta u - \dfrac{L}{2\rho c}\dfrac{\partial\phi}{\partial t}. \end{cases} \tag{2.1}$$

Taking the inner products of the above with $-\frac{\partial\phi}{\partial t}, \frac{\partial\phi}{\partial t}, 2r$ and $(\frac{2\rho c}{L})^2 u$ respectively, we obtain the modified energy dissipation law:

$$\frac{d}{dt}\tilde{E}(\phi,u,r) = -\left\|\sqrt{\tau}\frac{\partial\phi}{\partial t}\right\|^2 - K\big(\frac{2\rho c}{L}\big)^2\|\nabla u\|^2, \tag{2.2}$$

where $\tilde{E}(\phi,u,r) = \displaystyle\int_\Omega\left(\frac{\varepsilon^2}{2}|\nabla\phi|^2 + 2\big(\frac{\rho c}{L}\big)^2u^2\right)d\boldsymbol{x} + r^2.$

It is readily seen that according to the definition of the auxiliary variable $r(t)$ there is no essential difference between the energy laws (1.3) and (2.2) since the energy $E(\phi,u)$ and $\tilde{E}(\phi,u,r)$ are essentially same up to the constant C_0. This is a natural result since the reformulated equation set (2.1) is strictly equivalent to the original equation set (1.2). However, as we are going to see, at the discrete level the energy dissipation law will take the form (2.2) rather than (1.3).

In this section, we propose three schemes and carry out the stability analysis for each of these schemes. Let $n = 0, 1, \ldots$ be the time step, δt be the time step size, $t^n = n\delta t$.

2.1. **A first order scheme.** We begin with constructing a first order scheme based on the reformulated system (2.1) as follows:

$$\tau\frac{\phi^{n+1}-\phi^n}{\delta t}=-\sigma^{n+1}, \tag{2.3a}$$

$$\sigma^{n+1}=-\varepsilon^2\Delta\phi^{n+1}+\frac{r^{n+1}}{\sqrt{E_1(\phi^n)+C_0}}F'(\phi^n)-\frac{2\rho c}{L}u^{n+1}, \tag{2.3b}$$

$$\frac{r^{n+1}-r^n}{\delta t}=\frac{1}{2\sqrt{E_1(\phi^n)+C_0}}\int_\Omega F'(\phi^n)\frac{\phi^{n+1}-\phi^n}{\delta t}d\boldsymbol{x}, \tag{2.3c}$$

$$\frac{u^{n+1}-u^n}{\delta t}=K\Delta u^{n+1}-\frac{L}{2\rho c}\frac{\phi^{n+1}-\phi^n}{\delta t}, \tag{2.3d}$$

where ϕ^n is an approximation to $\phi(t^n)$. Intuitively, this is a first order scheme since it is a combination of the first order (at least) discretizations to different terms of the equations. However a rigorous proof of the convergence order remains an open question. Instead, we will provide a proof for the stability of the scheme, and the convergence order will be verified through the numerical experiments to be presented later on.

Theorem 2.1. *The scheme* (2.3) *is unconditionally stable in the sense that the following inequality holds for all* $n=0,1,\ldots$*:*

$$\begin{aligned}&\frac{\varepsilon^2}{2}\|\nabla\phi^{n+1}\|^2+2\big(\frac{\rho c}{L}\big)^2\|u^{n+1}\|^2+|r^{n+1}|^2 \\ -\Big[\frac{\varepsilon^2}{2}\|\nabla\phi^n\|^2+2\big(\frac{\rho c}{L}\big)^2\|u^n\|^2+|r^n|^2\Big]&\le-\delta t\left[\left\|\sqrt{\tau}\frac{\phi^{n+1}-\phi^n}{\delta t}\right\|^2+K\big(\frac{2\rho c}{L}\big)^2\|\nabla u^{n+1}\|^2\right],\end{aligned} \tag{2.4}$$

which means the solution remains bounded during the time stepping.

Proof. By taking the inner products of (2.3a)-(2.3d) with $-\frac{\phi^{n+1}-\phi^n}{\delta t}$, $\frac{\phi^{n+1}-\phi^n}{\delta t}$, $2r^{n+1}$, and $(\frac{2\rho c}{L})^2u^{n+1}$ respectively, we obtain:

$$\Big(\tau\frac{\phi^{n+1}-\phi^n}{\delta t},-\frac{\phi^{n+1}-\phi^n}{\delta t}\Big)=\Big(\sigma^{n+1},\frac{\phi^{n+1}-\phi^n}{\delta t}\Big),$$

$$\begin{aligned}\Big(\sigma^{n+1},\frac{\phi^{n+1}-\phi^n}{\delta t}\Big)&=\frac{\varepsilon^2}{\delta t}\big(\nabla\phi^{n+1},\nabla(\phi^{n+1}-\phi^n)\big)\\&\quad+\frac{r^{n+1}}{\sqrt{E_1(\phi^n)+C_0}}\Big(F'(\phi^n),\frac{\phi^{n+1}-\phi^n}{\delta t}\Big)-\frac{2\rho c}{L}\Big(u^{n+1},\frac{\phi^{n+1}-\phi^n}{\delta t}\Big),\end{aligned}$$

$$\frac{2r^{n+1}(r^{n+1}-r^n)}{\delta t}=\frac{r^{n+1}}{\sqrt{E_1(\phi^n)+C_0}}\Big(F'(\phi^n),\frac{\phi^{n+1}-\phi^n}{\delta t}\Big),$$

$$\frac{1}{\delta t}\big(\frac{2\rho c}{L}\big)^2(u^{n+1}-u^n,u^{n+1})=-K\big(\frac{2\rho c}{L}\big)^2(\nabla u^{n+1},\nabla u^{n+1})-\frac{2\rho c}{L}\Big(\frac{\phi^{n+1}-\phi^n}{\delta t},u^{n+1}\Big).$$

Combining the above four equalities and using the identity

$$2(a^{k+1},a^{k+1}-a^k)=|a^{k+1}|^2-|a^k|^2+|a^{k+1}-a^k|^2, \tag{2.5}$$

we have

$$\frac{\varepsilon^2}{2\delta t}(\|\nabla\phi^{n+1}\|^2-\|\nabla\phi^n\|^2+\|\nabla\phi^{n+1}-\nabla\phi^n\|^2)+\frac{1}{\delta t}(|r^{n+1}|^2-|r^n|^2+|r^{n+1}-r^n|^2) \quad (2.6)$$
$$+\frac{2}{\delta t}(\frac{\rho c}{L})^2(\|u^{n+1}\|^2-\|u^n\|^2+\|u^{n+1}-u^n\|^2)+K(\frac{2\rho c}{L})^2\|\nabla u^{n+1}\|^2=-\left\|\sqrt{\tau}\frac{\phi^{n+1}-\phi^n}{\delta t}\right\|^2.$$

Then dropping some uninfluential positive terms, we get immediately the desired inequality (2.4).

□

The proposed scheme is unconditionally stable as proved in Theorem 2.1. However it can not be said efficient unless it can be implemented efficiently. We will see that, even though the coupling terms are treated implicitly in the scheme, the resulting equations can be formulated into decoupled equations with constant coefficients to be solved at each time step. To see that, we first formally obtain u^{n+1} from (2.3d):

$$Au^{n+1}=\frac{1}{\delta t}u^n-\frac{L}{2\rho c}\frac{\phi^{n+1}-\phi^n}{\delta t} \quad \text{with } A=\frac{1}{\delta t}I-K\Delta. \quad (2.7)$$

where I is the identity operator. Then we eliminate σ^{n+1} from (2.3a) by using (2.3b), (2.3c) and (2.7), yielding

$$\tau\frac{\phi^{n+1}-\phi^n}{\delta t}-\varepsilon^2\Delta\phi^{n+1}+b^n\big(r^n+\frac{1}{2}(b^n,\phi^{n+1}-\phi^n)\big)=\frac{2\rho c}{L}A^{-1}\Big(\frac{1}{\delta t}u^n-\frac{L}{2\rho c}\frac{\phi^{n+1}-\phi^n}{\delta t}\Big), \quad (2.8)$$

where

$$b^n:=\frac{F'(\phi^n)}{\sqrt{E_1(\phi^n)+C_0}}.$$

A^{-1} is the inverse of A subject to the homogeneous Dirichlet or Neumann boundary condition. Furthermore, reformulating (2.8) gives

$$\begin{aligned}&\big(\frac{\tau}{\delta t}I-\varepsilon^2\Delta+\frac{1}{\delta t}A^{-1}\big)\phi^{n+1}+\frac{1}{2}b^n(b^n,\phi^{n+1}) \quad (2.9)\\ =\;&\frac{1}{\delta t}(\tau I+A^{-1})\phi^n+b^n\big(\frac{1}{2}(b^n,\phi^n)-r^n\big)+\frac{2\rho c}{L\delta t}A^{-1}u^n.\end{aligned}$$

Denoting the right hand side in (2.9) by g^n, then solving ϕ^{n+1} from (2.9) can be done in three steps as follows:

1) Solve ϕ_1^{n+1} from the equation

$$\Big(\frac{\tau}{\delta t}I-\varepsilon^2\Delta+\frac{1}{\delta t}A^{-1}\Big)\phi_1^{n+1}=-\frac{1}{2}b^n. \quad (2.10a)$$

2) Solve ϕ_2^{n+1} from the equation

$$\Big(\frac{\tau}{\delta t}I-\varepsilon^2\Delta+\frac{1}{\delta t}A^{-1}\Big)\phi_2^{n+1}=g^n. \quad (2.10b)$$

3) Set

$$\phi^{n+1}=(b^n,\phi^{n+1})\phi_1^{n+1}+\phi_2^{n+1}. \quad (2.10c)$$

Once ϕ^{n+1} is obtained, u^{n+1} will be computed from (2.7). It remains to show how to compute ϕ^{n+1} from the steps (2.10). While the equations governing ϕ_1^{n+1} and ϕ_2^{n+1}, i.e., (2.10a) and

(2.10b) are clear, it is not evident how to solve ϕ^{n+1} from (2.10c). To this end, we take the inner product of (2.10c) with b^n:

$$(b^n, \phi^{n+1}) + \gamma^n (b^n, \phi^{n+1}) = (b^n, \phi_2^{n+1}), \tag{2.11}$$

where

$$\gamma^n = -(b^n, \phi_1^{n+1}) = \Big(b^n, \frac{1}{2} B^{-1} b^n\Big) \ \text{ with } B = \frac{\tau}{\delta t} I - \varepsilon^2 \Delta + \frac{1}{\delta t} A^{-1}. \tag{2.12}$$

Since A^{-1} is a positive definite operator, B^{-1} is also a positive definite operator, thus $\gamma^n \geq 0$. Then it follows from (2.11) that

$$(b^n, \phi^{n+1}) = \frac{(b^n, \phi_2^{n+1})}{1 + \gamma^n}. \tag{2.13}$$

With (b^n, ϕ^{n+1}) computed by this expression, ϕ^{n+1} is obtained from (2.10c) directly.

To summarize, the scheme (2.3) can be easily implemented in the following manner:

(*i*) Calculate ϕ_1^{n+1} and ϕ_2^{n+1} by solving the two constant coefficient equations (2.10a) and (2.10b) respectively, which can be realized in parallel.

(*ii*) Compute (b^n, ϕ^{n+1}) by using (2.13), then ϕ^{n+1} using (2.10c).

(*iii*) Compute u^{n+1} by using (2.7).

Thus the total computational complexity at each time step is essentially solving several second-order elliptic problems with constant coefficients, for which there exist different fast solvers.

Remark 2.1. *The equations* (2.10a), (2.10b), *and* (2.11) *involve the inversion of the operator A, which is caused by the implicit treatment of the both coupling terms; i.e., the last two terms in* (2.3b) *and* (2.3d). *Generally, the presence of A^{-1} in the equations may make the computation expensive if an iterative method is considered to solve these equations since an inner-outer iteration loop becomes inevitable. However, as we are going to see, if a suitable discretization method in space is chosen, the equations* (2.10a), (2.10b), *and* (2.11) *can be very efficiently solved. A fast solver based on spectral methods will be detailed in the next section.*

Remark 2.2. *Alternatively, we can consider an explicit way to treat the coupling terms in* (2.1). *For example, we can explicitly treat the coupling term in the phase field equation, resulting in a scheme as follows:*

$$\tau \frac{\phi^{n+1} - \phi^n}{\delta t} = -\sigma^{n+1}, \tag{2.14a}$$

$$\sigma^{n+1} = -\varepsilon^2 \Delta \phi^{n+1} + \frac{r^{n+1}}{\sqrt{E_1(\phi^n) + C_0}} F'(\phi^n) - \frac{2\rho c}{L} u^n, \tag{2.14b}$$

$$\frac{r^{n+1} - r^n}{\delta t} = \frac{1}{2\sqrt{E_1(\phi^n) + C_0}} \int_\Omega F'(\phi^n) \frac{\phi^{n+1} - \phi^n}{\delta t} d\boldsymbol{x}, \tag{2.14c}$$

$$\frac{u^{n+1} - u^n}{\delta t} = K \Delta u^{n+1} - \frac{L}{2\rho c} \frac{\phi^{n+1} - \phi^n}{\delta t}. \tag{2.14d}$$

Notice that, as compared to the scheme (2.3), *the term $\frac{2\rho c}{L} u^{n+1}$ in* (2.3b) *is now replaced by $\frac{2\rho c}{L} u^n$ in* (2.14b). *Doing so allows to first compute ϕ^{n+1} directly by combining* (2.14a)-(2.14c)*:*

$$\Big(\frac{\tau}{\delta t} I - \varepsilon^2 \Delta\Big) \phi^{n+1} + \frac{1}{2} b^n (b^n, \phi^{n+1}) = \frac{\tau}{\delta t} \phi^n + b^n \Big(\frac{1}{2} (b^n, \phi^n) - r^n\Big) + \frac{2\rho c}{L} u^n. \tag{2.15}$$

Then compute u^{n+1} by using (2.14d)*. The scheme* (2.14) *is obviously easier to implement. The drawback of this scheme is that its stability is not demonstrable, at least for the time being. Nevertheless the stability property of the scheme will be numerically investigated later in the numerical test section.*

2.2. **A BDF-type second order scheme (BDF-2).** Now we construct a scheme for the system (2.1) using the backward differentiation formula of second order for the time derivatives and second order extrapolation for the nonlinear term:

$$\tau\frac{3\phi^{n+1}-4\phi^{n}+\phi^{n-1}}{2\delta t}=-\sigma^{n+1}, \tag{2.16a}$$

$$\sigma^{n+1}=-\varepsilon^2\Delta\phi^{n+1}+\frac{r^{n+1}}{\sqrt{E_1(\phi^{n+\frac{1}{2}})+C_0}}F'(\phi^{n+\frac{1}{2}})-\frac{2\rho c}{L}u^{n+1}, \tag{2.16b}$$

$$\frac{3r^{n+1}-4r^{n}+r^{n-1}}{2\delta t}=\frac{1}{2\sqrt{E_1(\phi^{n+\frac{1}{2}})+C_0}}\int_\Omega F'(\phi^{n+\frac{1}{2}})\frac{3\phi^{n+1}-4\phi^{n}+\phi^{n-1}}{2\delta t}d\boldsymbol{x}, \tag{2.16c}$$

$$\frac{3u^{n+1}-4u^{n}+u^{n-1}}{2\delta t}=K\Delta u^{n+1}-\frac{L}{2\rho c}\frac{3\phi^{n+1}-4\phi^{n}+\phi^{n-1}}{2\delta t}, \tag{2.16d}$$

where $\phi^{n+\frac{1}{2}}:=2\phi^n-\phi^{n-1}$. Formally this is a second order scheme, hereafter called as BDF-2. The stability of this scheme is established in the following theorem.

Theorem 2.2. *The solution of the scheme* (2.16) *satisfies:*

$$\begin{aligned}
&\frac{\varepsilon^2}{4}\left[(\|\nabla\phi^{n+1}\|^2+\|\nabla(2\phi^{n+1}-\phi^n)\|^2)-(\|\nabla\phi^n\|^2+\|\nabla(2\phi^n-\phi^{n-1})\|^2)\right] \\
&\quad+\big(\frac{\rho c}{L}\big)^2\left[(\|u^{n+1}\|^2+\|2u^{n+1}-u^n\|^2)-(\|u^n\|^2+\|2u^n-u^{n-1}\|^2)\right] \\
&\quad+\frac{1}{2}\left[(|r^{n+1}|^2+|2r^{n+1}-r^n|^2)-(|r^n|^2+|2r^n-r^{n-1}|^2)\right] \\
&\quad\le-\delta t\left[\left\|\sqrt{\tau}\frac{3\phi^{n+1}-4\phi^n+\phi^{n-1}}{2\delta t}\right\|^2+K\big(\frac{2\rho c}{L}\big)^2\|\nabla u^{n+1}\|^2\right].
\end{aligned} \tag{2.17}$$

Consequently $\frac{\varepsilon^2}{4}\big(\|\nabla\phi^{n+1}\|^2+\|\nabla(2\phi^{n+1}-\phi^n)\|^2\big)+\big(\frac{\rho c}{L}\big)^2\big(\|u^{n+1}\|^2+\|2u^{n+1}-u^n\|^2\big)+\frac{1}{2}\big(|r^{n+1}|^2+|2r^{n+1}-r^n|^2\big)$*, therefore* $\|\nabla\phi^{n+1}\|^2+\|u^{n+1}\|^2$*, is bounded for all* $n=0,1,\ldots$*. This means the scheme* (2.16) *is unconditionally stable.*

Proof. The proof makes use of the same idea as for Theorem 2.1. By taking the inner products of (2.16a)-(2.16d) with $-\frac{3\phi^{n+1}-4\phi^n+\phi^{n-1}}{2\delta t}$, $\frac{3\phi^{n+1}-4\phi^n+\phi^{n-1}}{2\delta t}$, $2r^{n+1}$, $(\frac{2\rho c}{L})^2u^{n+1}$ respectively, we obtain:

$$\Big(\tau\frac{3\phi^{n+1}-4\phi^n+\phi^{n-1}}{2\delta t},-\frac{3\phi^{n+1}-4\phi^n+\phi^{n-1}}{2\delta t}\Big)=(\sigma^{n+1},\frac{3\phi^{n+1}-4\phi^n+\phi^{n-1}}{2\delta t}),$$

$$\Big(\sigma^{n+1},\frac{3\phi^{n+1}-4\phi^n+\phi^{n-1}}{2\delta t}\Big)=\frac{\varepsilon^2}{2\delta t}\Big(\nabla\phi^{n+1},\nabla(3\phi^{n+1}-4\phi^n+\phi^{n-1})\Big)$$
$$+\frac{r^{n+1}}{\sqrt{E_1(\phi^{n+\frac12})+C_0}}\Big(F'(\phi^{n+\frac12}),\frac{3\phi^{n+1}-4\phi^n+\phi^{n-1}}{2\delta t}\Big)-\frac{2\rho c}{L}\Big(u^{n+1},\frac{3\phi^{n+1}-4\phi^n+\phi^{n-1}}{2\delta t}\Big),$$

$$\frac{2r^{n+1}(3r^{n+1}-4r^n+r^{n-1})}{2\delta t}=\frac{r^{n+1}}{\sqrt{E_1(\phi^{n+\frac12})+C_0}}\Big(F'(\phi^{n+\frac12}),\frac{3\phi^{n+1}-4\phi^n+\phi^{n-1}}{2\delta t}\Big),$$

$$\frac{1}{2\delta t}(\frac{2\rho c}{L})^2\Big(3u^{n+1}-4u^n+u^{n-1},u^{n+1}\Big)=-K(\frac{2\rho c}{L})^2(\nabla u^{n+1},\nabla u^{n+1})$$
$$-\frac{2\rho c}{L}\Big(\frac{3\phi^{n+1}-4\phi^n+\phi^{n-1}}{2\delta t},u^{n+1}\Big).$$

Then combining the above four equalities, using the identity

$$\begin{aligned}&2(a^{k+1},3a^{k+1}-4a^k+a^{k-1})\\&=|a^{k+1}|^2+|2a^{k+1}-a^k|^2-|a^k|^2-|2a^k-a^{k-1}|^2+|a^{k+1}-2a^k+a^{k-1}|^2,\end{aligned}\tag{2.18}$$

and dropping some uninfluential positive terms, we obtain the desired result (2.17). □

The implementation technique for the scheme (2.16) is similar to (2.3), which is described below. We first obtain u^{n+1} from (2.16d):

$$\bar{A}u^{n+1}=\frac{4u^n-u^{n-1}}{2\delta t}-\frac{L}{2\rho c}\frac{3\phi^{n+1}-4\phi^n+\phi^{n-1}}{2\delta t}\quad\text{with }\bar{A}=\frac{3}{2\delta t}I-K\Delta.\tag{2.19}$$

Then we eliminate σ^{n+1} from (2.16a) by using (2.16b), (2.16c), and (2.19) to obtain

$$\begin{aligned}\tau\frac{3\phi^{n+1}-4\phi^n+\phi^{n-1}}{2\delta t}-\varepsilon^2\Delta\phi^{n+1}+\frac13 b^{n+\frac12}\big(4r^n-r^{n-1}+\frac12(b^{n+\frac12},3\phi^{n+1}-4\phi^n+\phi^{n-1})\big)\\=\frac{2\rho c}{L}\bar{A}^{-1}\Big(\frac{4u^n-u^{n-1}}{2\delta t}-\frac{L}{2\rho c}\frac{3\phi^{n+1}-4\phi^n+\phi^{n-1}}{2\delta t}\Big),\end{aligned}\tag{2.20}$$

where

$$b^{n+\frac12}:=\frac{F'(\phi^{n+\frac12})}{\sqrt{E_1(\phi^{n+\frac12})+C_0}}.$$

Furthermore, reformulating (2.20) gives

$$\begin{aligned}\Big(\frac{3\tau}{2\delta t}I-\varepsilon^2\Delta+\frac{3}{2\delta t}\bar{A}^{-1}\Big)\phi^{n+1}+\frac12 b^{n+\frac12}(b^{n+\frac12},\phi^{n+1})=\frac{\tau I+\bar{A}^{-1}}{2\delta t}(4\phi^n-\phi^{n-1})\\+\frac13 b^{n+\frac12}\Big(\frac12(b^{n+\frac12},4\phi^n-\phi^{n-1})-(4r^n-r^{n-1})\Big)+\frac{\rho c\bar{A}^{-1}}{L\delta t}(4u^n-u^{n-1}).\end{aligned}\tag{2.21}$$

Denoting the right hand side in (2.21) $\bar{g}^n$, the above equation is equivalent to:

1) Solve ϕ_1^{n+1} from the equation

$$\Big(\frac{3\tau}{2\delta t}I - \varepsilon^2\Delta + \frac{3}{2\delta t}\bar{A}^{-1}\Big)\phi_1^{n+1} = -\frac{1}{2}b^{n+\frac{1}{2}}. \tag{2.22a}$$

2) Solve ϕ_2^{n+1} from the equation

$$\Big(\frac{3\tau}{2\delta t}I - \varepsilon^2\Delta + \frac{3}{2\delta t}\bar{A}^{-1}\Big)\phi_2^{n+1} = \bar{g}^n. \tag{2.22b}$$

3) Set

$$\phi^{n+1} = (b^{n+\frac{1}{2}}, \phi^{n+1})\phi_1^{n+1} + \phi_2^{n+1}. \tag{2.22c}$$

To see how ϕ^{n+1} can be computed from (2.22c) after calculating ϕ_1^{n+1} and ϕ_2^{n+1} from (2.22a) and (2.22b), we take the inner product of (2.22c) with $b^{n+\frac{1}{2}}$ to get

$$(b^{n+\frac{1}{2}}, \phi^{n+1}) + \gamma^n(b^{n+\frac{1}{2}}, \phi^{n+1}) = (b^{n+\frac{1}{2}}, \phi_2^{n+1}), \tag{2.23}$$

where

$$\gamma^n = -(b^{n+\frac{1}{2}}, \phi_1^{n+1}) = \Big(b^{n+\frac{1}{2}}, \frac{1}{2}\bar{B}^{-1}b^{n+\frac{1}{2}}\Big) \text{ with } \bar{B} = \frac{3\tau}{2\delta t}I - \varepsilon^2\Delta + \frac{3}{2\delta t}\bar{A}^{-1}. \tag{2.24}$$

γ^n is positive since $\bar{A}^{-1}$ and $\bar{B}^{-1}$ are both positive definite operators. Then it follows from (2.23) that

$$(b^{n+\frac{1}{2}}, \phi^{n+1}) = \frac{(b^{n+\frac{1}{2}}, \phi_2^{n+1})}{1+\gamma^n}. \tag{2.25}$$

Bringing (2.25) into (2.22c) with γ^n computed by (2.24) gives ϕ^{n+1} explicitly. Once ϕ^{n+1} is obtained from (2.22c), we compute u^{n+1} by using (2.19).

The algorithm of the second order scheme is summarized as follows:

(*i*) Calculate ϕ_1^{n+1} and ϕ_2^{n+1} by solving in parallel the two constant coefficient equations (2.22a) and (2.22b) respectively.

(*ii*) Compute $(b^{n+\frac{1}{2}}, \phi^{n+1})$ by using (2.25), then ϕ^{n+1} using (2.22c).

(*iii*) Compute u^{n+1} by using (2.16d).

2.3. **A Crank-Nicolson type second order scheme (CN2).** Alternatively a second order scheme can also be designed based on Crank-Nicolson formula for the auxiliary variable reformulation (2.1) as follows:

$$\tau\frac{\phi^{n+1}-\phi^n}{\delta t}=-\sigma^{n+\frac{1}{2}}, \tag{2.26a}$$

$$\sigma^{n+\frac{1}{2}}=-\varepsilon^2\frac{\Delta(\phi^{n+1}+\phi^n)}{2}+\frac{r^{n+1}+r^n}{2\sqrt{E_1(\widehat{\phi}^{n+\frac{1}{2}})+C_0}}F'(\widehat{\phi}^{n+\frac{1}{2}})-\frac{2\rho c}{L}\frac{u^{n+1}+u^n}{2}, \tag{2.26b}$$

$$\frac{r^{n+1}-r^n}{\delta t}=\frac{1}{2\sqrt{E_1(\widehat{\phi}^{n+\frac{1}{2}})+C_0}}\int_\Omega F'(\widehat{\phi}^{n+\frac{1}{2}})\frac{\phi^{n+1}-\phi^n}{\delta t}d\boldsymbol{x}, \tag{2.26c}$$

$$\frac{u^{n+1}-u^n}{\delta t}=K\frac{\Delta(u^{n+1}+u^n)}{2}-\frac{L}{2\rho c}\frac{\phi^{n+1}-\phi^n}{\delta t}, \tag{2.26d}$$

where $\widehat{\phi}^{n+\frac{1}{2}}:=\frac{3\phi^n-\phi^{n-1}}{2}$ is an explicit approximation to $\phi(t^{n+\frac{1}{2}})$.

The above scheme equally possesses the unconditional stability property as proved in the following theorem.

Theorem 2.3. *The scheme* (2.26) *is unconditionally stable in the sense that*

$$\begin{aligned}&\frac{\varepsilon^2}{2}(\|\nabla\phi^{n+1}\|^2-\|\nabla\phi^n\|^2)+2\big(\frac{\rho c}{L}\big)^2(\|u^{n+1}\|^2-\|u^n\|^2) \\ &+(|r^{n+1}|^2-|r^n|^2)=-\delta t\left[\left\|\sqrt{\tau}\frac{\phi^{n+1}-\phi^n}{\delta t}\right\|^2+K\big(\frac{\rho c}{L}\big)^2\|\nabla(u^{n+1}+u^n)\|^2\right],\end{aligned} \tag{2.27}$$

which implies that $\frac{\varepsilon^2}{2}\|\nabla\phi^{n+1}\|^2+2(\frac{\rho c}{L})^2\|u^{n+1}\|^2+|r^{n+1}|^2$*, consequently* $\|\nabla\phi^{n+1}\|^2+\|u^{n+1}\|^2$ *remains bounded during the time stepping.*

Proof. The proof follows the procedure as in the two previous theorems. Taking the L^2 inner products of (2.26a)-(2.26d) with $-\frac{\phi^{n+1}-\phi^n}{\delta t}$, $\frac{\phi^{n+1}-\phi^n}{\delta t}$, $r^{n+1}+r^n$, and $2(\frac{\rho c}{L})^2(u^{n+1}+u^n)$ respectively, we obtain:

$$\Big(\tau\frac{\phi^{n+1}-\phi^n}{\delta t},-\frac{\phi^{n+1}-\phi^n}{\delta t}\Big)=\Big(\sigma^{n+\frac{1}{2}},\frac{\phi^{n+1}-\phi^n}{\delta t}\Big),$$

$$\begin{aligned}\Big(\sigma^{n+\frac{1}{2}},\frac{\phi^{n+1}-\phi^n}{\delta t}\Big)&=\frac{\varepsilon^2}{2\delta t}\Big(\nabla(\phi^{n+1}+\phi^n),\nabla(\phi^{n+1}-\phi^n)\Big)\\&+\frac{r^{n+1}+r^n}{2\sqrt{E_1(\widehat{\phi}^{n+\frac{1}{2}})+C_0}}\Big(F'(\widehat{\phi}^{n+\frac{1}{2}}),\frac{\phi^{n+1}-\phi^n}{\delta t}\Big)-\frac{2\rho c}{L}\Big(\frac{u^{n+1}+u^n}{2},\frac{\phi^{n+1}-\phi^n}{\delta t}\Big),\end{aligned}$$

$$\frac{(r^{n+1}+r^n)(r^{n+1}-r^n)}{\delta t}=\frac{r^{n+1}+r^n}{2\sqrt{E_1(\widehat{\phi}^{n+\frac{1}{2}})+C_0}}\Big(F'(\widehat{\phi}^{n+\frac{1}{2}}),\frac{\phi^{n+1}-\phi^n}{\delta t}\Big),$$

$$\begin{aligned}\frac{1}{\delta t}(\frac{2\rho c}{L})^2\Big(u^{n+1}-u^n,\frac{u^{n+1}+u^n}{2}\Big)&=-K(\frac{\rho c}{L})^2(\nabla(u^{n+1}+u^n),\nabla(u^{n+1}+u^n))\\&-\frac{2\rho c}{L}\Big(\frac{\phi^{n+1}-\phi^n}{\delta t},\frac{u^{n+1}+u^n}{2}\Big).\end{aligned}$$

Then we put all above equalities together to conclude. □

The implementation of the CN2 scheme is briefly described below. First formally it follows from (2.26d):

$$\tilde{A}u^{n+1} = \Big(\frac{1}{\delta t}I + \frac{K}{2}\Delta\Big)u^n - \frac{L}{2\rho c}\frac{\phi^{n+1}-\phi^n}{\delta t} \quad \text{with } \tilde{A} = \frac{1}{\delta t}I - \frac{K}{2}\Delta. \tag{2.28}$$

Then we eliminate σ^{n+1} from (2.26a) by using (2.26b), (2.26c), and (2.28) to obtain the equation for ϕ^{n+1}:

$$\begin{aligned}\tau\frac{\phi^{n+1}-\phi^n}{\delta t} - \varepsilon^2\frac{\Delta(\phi^{n+1}+\phi^n)}{2} + \frac{1}{2}\widehat{b}^{n+\frac{1}{2}}\Big(2r^n + \frac{1}{2}(\widehat{b}^{n+\frac{1}{2}}, \phi^{n+1}-\phi^n)\Big) \\ = \frac{\rho c}{L}\Big(\tilde{A}^{-1}\Big((\frac{1}{\delta t}I + \frac{K}{2}\Delta)u^n - \frac{L}{2\rho c}\frac{\phi^{n+1}-\phi^n}{\delta t}\Big) + u^n\Big),\end{aligned} \tag{2.29}$$

where

$$\widehat{b}^{n+\frac{1}{2}} := \frac{F'(\widehat{\phi}^{n+\frac{1}{2}})}{\sqrt{E_1(\widehat{\phi}^{n+\frac{1}{2}}) + C_0}}.$$

Rearranging (2.29) gives

$$\begin{aligned}&\Big(\frac{\tau}{\delta t}I - \frac{\varepsilon^2}{2}\Delta + \frac{\tilde{A}^{-1}}{2\delta t}\Big)\phi^{n+1} + \frac{1}{4}\widehat{b}^{n+\frac{1}{2}}(\widehat{b}^{n+\frac{1}{2}}, \phi^{n+1}) \\ = \ &\Big(\frac{\tau}{\delta t}I + \frac{\varepsilon^2}{2}\Delta + \frac{\tilde{A}^{-1}}{2\delta t}\Big)\phi^n + \widehat{b}^{n+\frac{1}{2}}\big(\frac{1}{4}(\widehat{b}^{n+\frac{1}{2}}, \phi^n) - r^n\big) + \frac{\rho c}{L}\Big(\tilde{A}^{-1}\big(\frac{1}{\delta t}I + \frac{K}{2}\Delta\big) + I\Big)u^n.\end{aligned} \tag{2.30}$$

Let $\tilde{g}^n$ denote the right hand side in (2.30), then the above equation is equivalent to:

1) Solve ϕ_1^{n+1} from the equation

$$\Big(\frac{\tau}{\delta t}I - \frac{\varepsilon^2}{2}\Delta + \frac{1}{2\delta t}\tilde{A}^{-1}\Big)\phi_1^{n+1} = -\frac{1}{4}\widehat{b}^{n+\frac{1}{2}}, \tag{2.31a}$$

2) Solve ϕ_2^{n+1} from the equation

$$\Big(\frac{\tau}{\delta t}I - \frac{\varepsilon^2}{2}\Delta + \frac{1}{2\delta t}\tilde{A}^{-1}\Big)\phi_2^{n+1} = \tilde{g}^n, \tag{2.31b}$$

3) Set

$$\phi^{n+1} = (\widehat{b}^{n+\frac{1}{2}}, \phi^{n+1})\phi_1^{n+1} + \phi_2^{n+1}. \tag{2.31c}$$

Using the technique we presented before, the computation of ϕ^{n+1} can be realized in an efficient way. Once this is done, we return to (2.28) to compute u^{n+1}.

Similar to Remark 2.2, second order easier-to-implement schemes can also be constructed by considering explicit treatment for one of the coupling terms.

3. Spectral discretization in space and faster solver

This section is devoted to present a spectral method for the discretization in space and propose fast solver for the full discrete problem. In order to illustrate the basic idea, we only consider the first order scheme (2.3). The other two schemes can be performed in a similar way. In this case we will meet a number of second order differential equations at each time step. We will describe their discretization in details.

3.1. **Choice of basis functions.** The spectral method consists in approximating the solution by a polynomial. For the convenience of calculation, we set $\Omega = [-1,1]^2$, and denote $I\!P_N(\Omega)$ the space of polynomials of degree $\leq N$ in each direction. We will consider appropriate modal basis functions according to the used boundary conditions; see, e.g., [26].

- *Dirichlet boundary condition.*

In the case of homogeneous Dirichlet condition $\phi|_{\partial\Omega} = u|_{\partial\Omega} = 0$, the simplest choice is $\{h_k(x)h_l(y)\}_{k,l=0}^{N-2}$ as a basis of $\{v \in I\!P_N(\Omega), v|_{\partial\Omega} = 0\}$ for both phase field and temperature, where $h_k(x) = L_k(x) - L_{k+2}(x)$ with $L_k(x)$ being the Legendre polynomial of degree k.

- *Neumann boundary condition.*

Under the homogeneous Neumann condition, we define $\bar{h}_k(x) = L_k(x) - \frac{k(k+1)}{(k+2)(k+3)}L_{k+2}(x)$. Then $\bar{h}_k(x)$ satisfies $\bar{h}_k'(\pm 1) = 0$, and $\{\bar{h}_k(x)\bar{h}_l(y)\}_{k,l=0}^{N-2}$ forms a basis of $\{v \in I\!P_N(\Omega), \frac{\partial v}{\partial \boldsymbol{n}}|_{\partial\Omega} = 0\}$.

3.2. **Some useful matrix expressions.** We now give some useful matrix expressions that will be used in the subsequent calculations. Let $M_{kl} = (h_l, h_k), S_{kl} = (h_l', h_k'), \bar{M}_{kl} = (\bar{h}_l, \bar{h}_k), \bar{S}_{kl} = (\bar{h}_l', \bar{h}_k')$. Then the matrices S and $\bar{S}$ are diagonal with

$$
\begin{aligned}
S_{kk} &= (4k+6), && k = 0, 1, \cdots \\
\bar{S}_{kk} &= \frac{k(k+1)(4k+6)}{(k+2)(k+3)}, && k = 0, 1, \cdots
\end{aligned}
$$

The matrices M and $\bar{M}$ are symmetric penta-diagonal whose nonzero elements are

$$
M_{kl} = M_{lk} = \begin{cases} \dfrac{2}{2k+1} + \dfrac{2}{2k+5}, & l = k, \\ -\dfrac{2}{2k+5}, & l = k+2. \end{cases}
$$

$$
\bar{M}_{kl} = \bar{M}_{lk} = \begin{cases} \dfrac{2}{2k+1} + \dfrac{2k^2(k+1)^2}{(2k+5)(k+2)^2(k+3)^2}, & l = k, \\ -\dfrac{2k(k+1)}{(k+2)(k+3)(2k+5)}, & l = k+2, \end{cases}
$$

3.3. **Spectral method.** In this subsection, we propose a Galerkin spectral method for the spatial discretization of the equations resulted from the time stepping schemes. To fix the idea, let's consider the equations (2.10) subject to the homogeneous Dirichlet boundary condition for both ϕ and u.

We define the approximation space $S_N = \{v \in I\!P_N(\Omega), v|_{\partial\Omega} = 0\}$. Let $\gamma_i^{n+1} = A^{-1}\phi_i^{n+1}, i = 1, 2$. The Galerkin spectral method for the equations (2.10) reads: find $\phi_{1,N}^{n+1}, \phi_{2,N}^{n+1}, \gamma_{1,N}^{n+1}, \gamma_{2,N}^{n+1} \in S_N(\Omega)$, such that for all $q_N \in S_N(\Omega)$,

$$
\frac{\tau}{\delta t}(\phi_{1,N}^{n+1}, q_N) + \varepsilon^2(\nabla\phi_{1,N}^{n+1}, \nabla q_N) + \frac{1}{\delta t}(\gamma_{1,N}^{n+1}, q_N) = -\frac{1}{2}(b^n, q_N), \tag{3.1a}
$$

$$
\frac{\tau}{\delta t}(\phi_{2,N}^{n+1}, q_N) + \varepsilon^2(\nabla\phi_{2,N}^{n+1}, \nabla q_N) + \frac{1}{\delta t}(\gamma_{2,N}^{n+1}, q_N) = (g^n, q_N), \tag{3.1b}
$$

$$
\phi_N^{n+1} = \big(b^n, \phi_N^{n+1}\big)\phi_{1,N}^{n+1} + \phi_{2,N}^{n+1}. \tag{3.1c}
$$

The matrix form of the above problems can be obtained by expressing the numerical solutions $\phi_{i,N}^{n+1}, \gamma_{i,N}^{n+1}, i = 1, 2$, under

$$\phi_{i,N}^{n+1} = \sum_{k,l=0}^{N-2} \hat{\phi}_{i,k,l}^{n+1} h_k(x) h_l(y), \tag{3.2}$$
$$\gamma_{i,N}^{n+1} = \sum_{k,l=0}^{N-2} \hat{\gamma}_{i,k,l}^{n+1} h_k(x) h_l(y).$$

If we denote the unknown matrices Φ_i^{n+1} and $\Upsilon_i^{n+1}, i = 1, 2$, by $\left(\Phi_i^{n+1}\right)_{k,l} = \hat{\phi}_{i,k,l}^{n+1}$ and $\left(\Upsilon_i^{n+1}\right)_{k,l} = \hat{\gamma}_{i,k,l}^{n+1}$, then we deduce from (3.1) the following linear system:

$$\begin{cases} \dfrac{\tau}{\delta t} M\Phi_1^{n+1} M + \varepsilon^2 (S\Phi_1^{n+1} M + M\Phi_1^{n+1} S) + \dfrac{1}{\delta t} M\Upsilon_1^{n+1} M = B^n, \\ \dfrac{\tau}{\delta t} M\Phi_2^{n+1} M + \varepsilon^2 (S\Phi_2^{n+1} M + M\Phi_2^{n+1} S) + \dfrac{1}{\delta t} M\Upsilon_2^{n+1} M = G^n, \end{cases} \tag{3.3}$$

where

$$\left(B^n\right)_{k,l} = -\frac{1}{2}(b^n, h_k(x)h_l(y)), \quad \left(G^n\right)_{k,l} = (g^n, h_k(x)h_l(y)),$$

the matrices M and S are defined in Subsection 3.2. We already know that the matrix M is symmetric pentadiagonal and S is diagonal, thus the linear system (3.3) can be solved by using a matrix diagonalization method, which we briefly describe below. Let Λ be the diagonal matrix whose diagonal entries $\{\lambda_k\}_{k=0}^{N-2}$ are the eigenvalues of $M^{-1}S$, and E be the matrix formed by the corresponding eigenvectors of $M^{-1}S$, i.e.,

$$M^{-1}SE = E\Lambda. \tag{3.4}$$

Note that all the eigenvalues are real and positive, E is a real matrix since M and S are both symmetric and positive definite matrices. Let $\widetilde{\Phi}_i^{n+1}$ and $\widetilde{\Upsilon}_i^{n+1}, i = 1, 2$ be the matrices such that $\Phi_i^{n+1} = E\widetilde{\Phi}_i^{n+1} E^T, \Upsilon_i^{n+1} = E\widetilde{\Upsilon}_i^{n+1} E^T$. Then (3.3) can be rewritten as

$$\begin{cases} \dfrac{\tau}{\delta t} ME\widetilde{\Phi}_1^{n+1} E^T M + \varepsilon^2 (SE\widetilde{\Phi}_1^{n+1} E^T M + ME\widetilde{\Phi}_1^{n+1} E^T S) + \dfrac{1}{\delta t} ME\widetilde{\Upsilon}_1^{n+1} E^T M = B^n, \\ \dfrac{\tau}{\delta t} ME\widetilde{\Phi}_2^{n+1} E^T M + \varepsilon^2 (SE\widetilde{\Phi}_2^{n+1} E^T M + ME\widetilde{\Phi}_2^{n+1} E^T S) + \dfrac{1}{\delta t} ME\widetilde{\Upsilon}_2^{n+1} E^T M = G^n. \end{cases} \tag{3.5}$$

Multiplying the left (resp. right) of the above equation by $(ME)^{-1}$ (resp. $(ME)^{-T}$) and using (3.4), the system (3.5) becomes

$$\begin{cases} \dfrac{\tau}{\delta t} \widetilde{\Phi}_1^{n+1} + \varepsilon^2 (\Lambda\widetilde{\Phi}_1^{n+1} + \widetilde{\Phi}_1^{n+1}\Lambda^T) + \dfrac{1}{\delta t} \widetilde{\Upsilon}_1^{n+1} = (ME)^{-1} B^n (ME)^{-T} := \widetilde{B}^n, \\ \dfrac{\tau}{\delta t} \widetilde{\Phi}_2^{n+1} + \varepsilon^2 (\Lambda\widetilde{\Phi}_2^{n+1} + \widetilde{\Phi}_2^{n+1}\Lambda^T) + \dfrac{1}{\delta t} \widetilde{\Upsilon}_2^{n+1} = (ME)^{-1} G^n (ME)^{-T} := \widetilde{G}^n, \end{cases} \tag{3.6}$$

which is equivalent to

$$\begin{cases} \dfrac{\tau}{\delta t} (\widetilde{\Phi}_1^{n+1})_{k,l} + \varepsilon^2 (\lambda_k + \lambda_l)(\widetilde{\Phi}_1^{n+1})_{k,l} + \dfrac{1}{\delta t} (\widetilde{\Upsilon}_1^{n+1})_{k,l} = (\widetilde{B}^n)_{k,l}, \\ \dfrac{\tau}{\delta t} (\widetilde{\Phi}_2^{n+1})_{k,l} + \varepsilon^2 (\lambda_k + \lambda_l)(\widetilde{\Phi}_2^{n+1})_{k,l} + \dfrac{1}{\delta t} (\widetilde{\Upsilon}_2^{n+1})_{k,l} = (\widetilde{G}^n)_{k,l}, \end{cases} \tag{3.7}$$

for all $k, l = 0, 1, \ldots, N-2$.
Remember that $\widetilde{\Upsilon}_i^{n+1}$ and $\widetilde{\Phi}_i^{n+1}$ are not independent unknowns. By definition, they are connected through $\gamma_i^{n+1} = A^{-1}\phi_i^{n+1}$, i.e.,

$$\phi_i^{n+1} = A\gamma_i^{n+1} = (\frac{1}{\delta t}I - K\Delta)\gamma_i^{n+1} = \frac{1}{\delta t}\gamma_i^{n+1} - K\Delta\gamma_i^{n+1}. \tag{3.8}$$

Their spectral approximations, i.e., $\phi_{i,N}^{n+1}$ and $\gamma_{i,N}^{n+1}$, satisfy the following Galerkin weak form:

$$(\phi_{i,N}^{n+1}, q_N) = \frac{1}{\delta t}(\gamma_{i,N}^{n+1}, q_N) + K(\nabla\gamma_{i,N}^{n+1}, \nabla q_N), \quad \forall q_N \in S_N(\Omega). \tag{3.9}$$

Processing as before, we get the relationship for their expansion coefficients $\widetilde{\Phi}_i^{n+1}$ and $\widetilde{\Upsilon}_i^{n+1}$ under the modal basis $\{h_k(x)h_l(y)\}_{k,l=0}^{N-2}$:

$$(\widetilde{\Upsilon}_i^{n+1})_{k,l} = \frac{\delta t}{1 + \delta t K(\lambda_k + \lambda_l)}(\widetilde{\Phi}_i^{n+1})_{k,l}, \quad k, l = 0, \ldots, N-2. \tag{3.10}$$

Substituting (3.10) into (3.7), we obtain

$$\begin{cases} \frac{\tau}{\delta t}(\widetilde{\Phi}_1^{n+1})_{k,l} + \varepsilon^2(\lambda_k + \lambda_l)(\widetilde{\Phi}_1^{n+1})_{k,l} + \frac{1}{1 + \delta t K(\lambda_k + \lambda_l)}(\widetilde{\Phi}_1^{n+1})_{k,l} = (\widetilde{B}^n)_{k,l}, \\ \frac{\tau}{\delta t}(\widetilde{\Phi}_2^{n+1})_{k,l} + \varepsilon^2(\lambda_k + \lambda_l)(\widetilde{\Phi}_2^{n+1})_{k,l} + \frac{1}{1 + \delta t K(\lambda_k + \lambda_l)}(\widetilde{\Phi}_2^{n+1})_{k,l} = (\widetilde{G}^n)_{k,l}. \end{cases} \tag{3.11}$$

Therefore,

$$\begin{aligned} \Big(\frac{\tau}{\delta t} + \varepsilon^2(\lambda_k + \lambda_l) + \frac{1}{1 + \delta t K(\lambda_k + \lambda_l)}\Big)(\widetilde{\Phi}_1^{n+1})_{k,l} = (\widetilde{B}^n)_{k,l}, \\ \Big(\frac{\tau}{\delta t} + \varepsilon^2(\lambda_k + \lambda_l) + \frac{1}{1 + \delta t K(\lambda_k + \lambda_l)}\Big)(\widetilde{\Phi}_2^{n+1})_{k,l} = (\widetilde{G}^n)_{k,l}. \end{aligned} \tag{3.12}$$

Using $\Phi_i^{n+1} = E\widetilde{\Phi}_i^{n+1}E^T$ we obtain the representation of the solution in the spectral space. Then we apply (3.2) to transform from the spectral space to the physical space, yielding the solutions $\phi_{1,N}^{n+1}$ and $\phi_{2,N}^{n+1}$. Then ϕ_N^{n+1} follows from (3.1c) using the formula (2.13). Finally, with ϕ_N^{n+1} obtained, the polynomial approximation u_N^{n+1} to u^{n+1} is constructed by the spectral discretization to (2.7): find $u_N^{n+1} \in S_N(\Omega)$ such that for all $w_N \in S_N(\Omega)$,

$$\frac{1}{\delta t}(u_N^{n+1}, w_N) + K(\nabla u_N^{n+1}, \nabla w_N) = (g_N^{n+1}, w_N), \tag{3.13}$$

where

$$g_N = \frac{1}{\delta t}u_N^n - \frac{L}{2\rho c}\frac{\phi_N^{n+1} - \phi_N^n}{\delta t}. \tag{3.14}$$

The matrix form of (3.13) with the spectral expansion

$$u_N^{n+1} = \sum_{k,l=0}^{N-2} \hat{u}_{k,l}^{n+1} h_k(x)h_l(y) \tag{3.15}$$

reads

$$\frac{1}{\delta t}MU^{n+1}M + K(MU^{n+1}S + SU^{n+1}M) = G_u^{n+1}, \tag{3.16}$$

where $\big(U^{n+1}\big)_{k,l} = \hat{u}_{k,l}^{n+1}$, $\big(G_u^{n+1}\big)_{k,l} = (g_N^{n+1}, h_k(x)h_l(y))$. Let $\widetilde{U}^{n+1}$ be the matrix such that $U^{n+1} = E\widetilde{U}^{n+1}E^T$, then (3.16) can be rewritten as

$$\frac{1}{\delta t}ME\widetilde{U}^{n+1}E^TM + K(SE\widetilde{U}^{n+1}E^TM + ME\widetilde{U}^{n+1}E^TS) = G_u^{n+1}. \tag{3.17}$$

Multiplying the left (resp. right) of the above equation by $(ME)^{-1}$ (resp. $(ME)^{-T}$) and using (3.4), the system (3.17) becomes

$$\frac{1}{\delta t}\widetilde{U}^{n+1} + K(\Lambda\widetilde{U}^{n+1} + \widetilde{U}^{n+1}\Lambda^T) = (ME)^{-1}G_u^{n+1}(ME)^{-T} := \widetilde{G}_u^{n+1}, \tag{3.18}$$

or, equivalently, for all $k, l = 0, \ldots, N-2$,

$$\frac{1}{\delta t}(\widetilde{U}^{n+1})_{k,l} + K(\lambda_k + \lambda_l)(\widetilde{U}^{n+1})_{k,l} = (\widetilde{G}_u^{n+1})_{k,l}. \tag{3.19}$$

That is,

$$\Big(\frac{1}{\delta t} + K(\lambda_k + \lambda_l)\Big)(\widetilde{U}^{n+1})_{k,l} = (\widetilde{G}_u^{n+1})_{k,l}. \tag{3.20}$$

The overall algorithm of the spectral fast solver for the first order scheme (2.3) is summarized below.

(i) Pre-processing: Compute the eigenvalues and eigenvectors of $M^{-1}S$ and form the matrix $(ME)^{-1}$.

(ii) Compute $\widetilde{B}^n := (ME)^{-1}B^n(ME)^{-T}$ and $\widetilde{G}^n := (ME)^{-1}G^n(ME)^{-T}$.

(iii) Obtain $\widetilde{\Phi}_i^{n+1}$, $i = 1, 2$, from (3.12) and set $\Phi_i^{n+1} = E\widetilde{\Phi}_i^{n+1}E^T$.

(iv) Get $\phi_{1,N}^{n+1}$ and $\phi_{2,N}^{n+1}$ from (3.2), then compute ϕ_N^{n+1} through (3.1c).

(v) Compute $\widetilde{G}_u^{n+1} := (ME)^{-1}G_u^{n+1}(ME)^{-T}$.

(vi) Obtain $\widetilde{U}^{n+1}$ from (3.20) and set $U^{n+1} = E\widetilde{U}^{n+1}E^T$.

(vii) Get u_N^{n+1} from (3.15).

Remark 3.1. *The case of the Neumann boundary condition can be handled in an exactly same way. It suffices to replace the approximation space by* $S_N = \{v \in I\!P_N(\Omega), \frac{\partial v}{\partial \boldsymbol{n}}|_{\partial\Omega} = 0\}$, *and the corresponding matrices* M *and* S *by* $\bar{M}$ *and* $\bar{S}$ *respectively. For the case of mixed boundary conditions, i.e., Dirichlet condition for* u *and Neumann boundary condition for* ϕ *there is no fast solver available for* (2.10) *since the connection between* $\widetilde{\Upsilon}_i^{n+1}$ *and* $\widetilde{\Phi}_i^{n+1}$ *in* (3.7) *is full. In this case, iterative methods can be suggested for solving* (2.10). *For example, we may consider the following Picard iteration:*

$$\begin{aligned}
\big(\frac{\tau}{\delta t}I - \varepsilon^2\Delta\big)\phi_1^{n+1,j+1} &= -\frac{1}{2}b^n - \frac{1}{\delta t}A^{-1}\phi_1^{n+1,j}, \\
\big(\frac{\tau}{\delta t}I - \varepsilon^2\Delta\big)\phi_2^{n+1,j+1} &= g^n - \frac{1}{\delta t}A^{-1}\phi_2^{n+1,j},
\end{aligned} \tag{3.21}$$

where $j = 0, 1, 2, \ldots$ *is the iteration number. The initial value* $\phi_i^{n+1,0}$ *can be chosen as* ϕ_i^n, *and the criterion to stop the iteration can be* $\dfrac{\|\phi_i^{n+1,j+1} - \phi_i^{n+1,j}\|}{\|\phi_i^{n+1,j+1}\|} \le tol$ *for a small enough tol,* $i = 1, 2$. *With the right side known, a fast solver is still available to compute* $\phi_i^{n+1,j+1}$ *from* (3.21).

4. Numerical results

In this section, we will present some numerical examples to demonstrate the stability and accuracy of the proposed schemes for the thermal phase change model. We begin with some smooth fabricated solutions, which is not real thermal phase change problem, but serve as accuracy measure.

Example 4.1. *(Convergence order test) We first consider the equation with the homogeneous Dirichlet boundary condition:*

$$\begin{cases} \tau\dfrac{\partial\phi}{\partial t} = \varepsilon^2\Delta\phi - \dfrac{1}{2}\phi(\phi^2-1) + \dfrac{2\rho c}{L}u + s_1(\boldsymbol{x},t), \quad \text{in } (-1,1)^2\times(0,T], \\ \dfrac{\partial u}{\partial t} = K\Delta u - \dfrac{L}{2\rho c}\dfrac{\partial\phi}{\partial t} + s_2(\boldsymbol{x},t) \quad \text{in } (-1,1)^2\times(0,T], \\ \phi(\boldsymbol{x},0) = u(\boldsymbol{x},0) = 0, \quad \forall \boldsymbol{x}\in(-1,1)^2, \end{cases} \tag{4.1}$$

where $s_1(\boldsymbol{x},t)$ and $s_2(\boldsymbol{x},t)$ are the fabricated source terms chosen such that the problem (4.1) *admits the exact solution as follows:*

$$\begin{cases} \phi(\boldsymbol{x},t) = \sin(t)\sin(\pi x)\sin(\pi y), \\ u(\boldsymbol{x},t) = \sin(t)\cos(\frac{\pi}{2}x)\cos(\frac{\pi}{2}y). \end{cases}$$

The purpose of this example is to verify the time and space convergence order of the proposed three schemes. We first investigate the time accuracy. The spatial discretization makes use of the Galerkin spectral method described in subsection 3.3 with mode number $N = 20$, which is large enough such that the spatial discretization error is negligible compared with the time error. The parameters used in this example are: $\rho = c = L = K = 1$. Note that in practical physical problems, the parameters τ and ε are usually small, which may cause difficulties in calculation. The first test also concerns the impact of τ and ε on the accuracy of the numerical solutions. In Figure 1 we present the L^2-errors at $T = 0.1$ as functions of the time step size δt in log-log scale for the first order scheme (2.10), BDF-2 scheme (2.22), and CN2 scheme (2.31). A comparison between $\tau = 1, \varepsilon^2 = 0.01$ and $\tau = 5e-3, \varepsilon^2 = 1e-4$ is shown in the figure. The left figures and the right figures are related to phase field ϕ and temperature u respectively, it is clearly observed that all three schemes achieve the expected convergence rates. Also observed is: for smaller τ and ε the expected convergence rates can only be reached when δt is small enough. What's more, compared with the larger τ and ε, the error with the smaller τ and ε is obviously bigger, and the difference is about 2 orders of magnitude.

We then investigate the spatial accuracy by examining the error behavior of the numerical solutions with respect to the polynomial degree N. The obtained results at $T = 0.1$ with the time step size $\delta t = 5e-6$ are shown in Figure 2. The L^2-errors curve for both phase field ϕ and temperature u are approximately linear (up to a level dominated by the temporal error) with respect to the polynomial degree N in semi-log scale. This is indicative of the exponential convergence.

We will end the investigation of this example by proving the stability of our scheme to handle the long times computational. We numerically test this long-term stability by using the BDF-2 scheme for the time discretization and Galerkin spectral method with $N = 256$ for the spatial

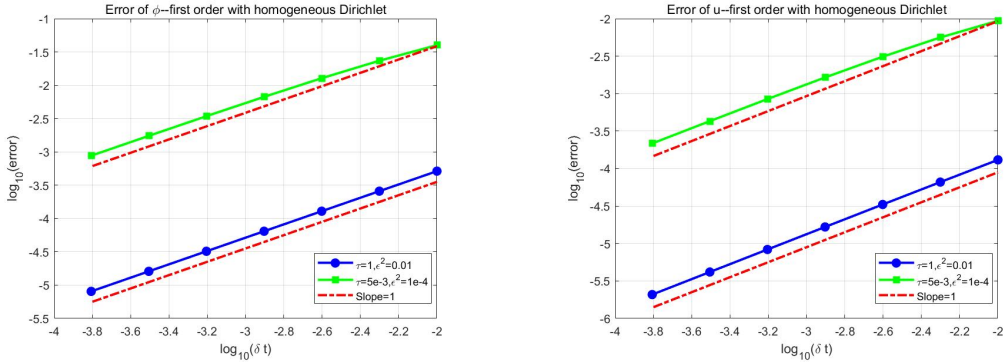

(a) error of ϕ (b) error of u

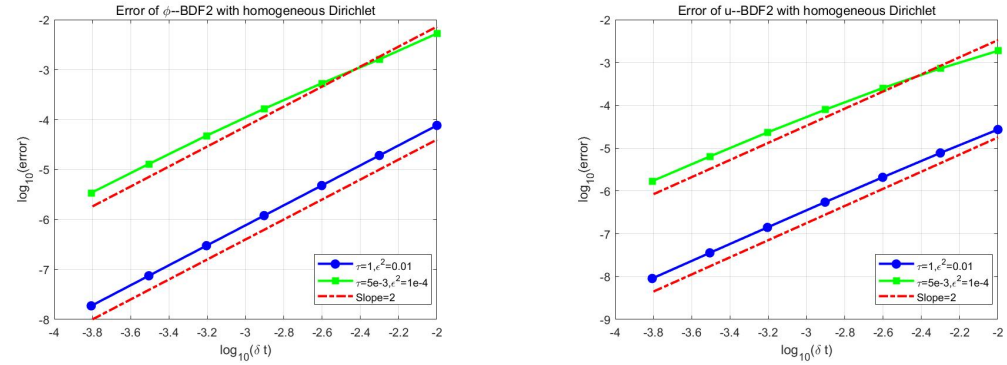

(c) error of ϕ (d) error of u

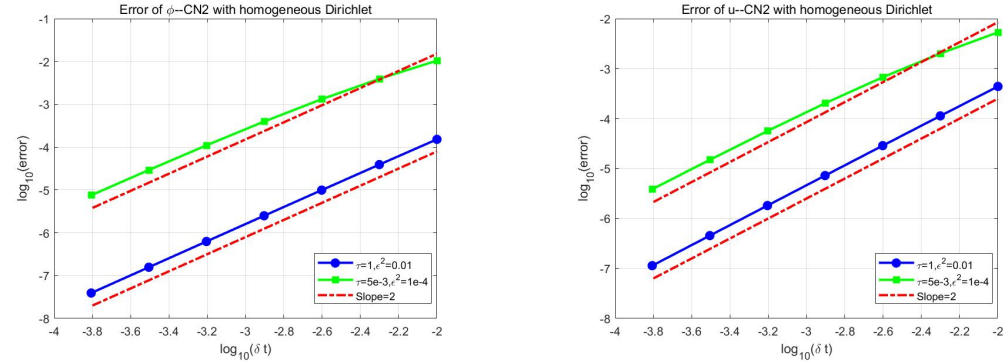

(e) error of ϕ (f) error of u

FIGURE 1. (Example 4.1) The error decay at $T = 0.1$ versus the time step sizes for the first order scheme ((a) and (b)), BDF-2 scheme ((c) and (d)) and CN2 scheme ((e) and (f)).

discretization. The parameters chosen in this example are: $\tau = \rho = c = L = K = \varepsilon^2 = 1$. The comparison between the exact solution and the results we calculated with $\delta t = 0.5$ at $t = 1, 500, 1000, 1500, 2000$ is displayed in the Figure 3. We can see that the ϕ and u we calculated in Figure 3(a) and (c) is equal to the exact solution ϕ and u we gave in Figure 3(b) and (d). So we can conclude that the scheme allow us to use large time step for long-term simulation.

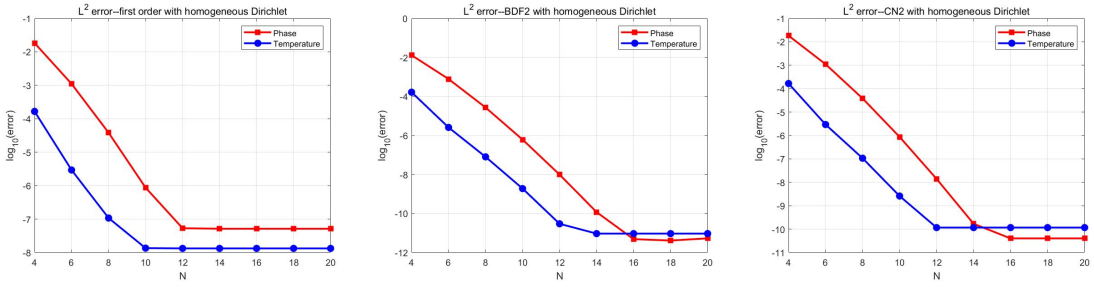

(a) first order scheme (b) BDF-2 scheme (c) CN2 scheme

FIGURE 2. (Example 4.1) The error decay at $T = 0.1$ versus the degree of polynomial N for the first order scheme (a), BDF-2 scheme (b) and CN2 scheme (c).

Example 4.2. *(Comparison of explicit and implicit schemes) As discussed in Remark 2.2, we aim at numerically investigating the stability property of the explicit scheme* (2.14) *and its second order counterparts. On the basis of the previous example, the numerical investigation is carried out by comparing the explicit and implicit treatment of the coupling term* $\frac{2\rho c}{L}u$ *in the equation* (2.1)*. Precisely, we will compare the stability between the schemes* (2.3) *and* (2.14)*, and between their higher order counterparts.*

We use the same equations, initial values, boundary conditions, and exact solutions as in Example 4.1. The difference is that the errors are evaluated at $T = 10$ in this example instead of $T = 1$ in Example 4.1. The obtained results are presented in Tables 1-3 for the first order scheme, BDF-2 scheme, and CN2 scheme respectively. It is seen that for all three schemes, the error of the implicit type is slightly smaller than that of the explicit one, while the implicit and explicit schemes achieve almost same convergence order. It is worth pointing out again that the explicit schemes are easier to implement, but there is no theoretical guarantee for their unconditional stability, although there is no observed instability neither in our numerical calculation for the tested parameters.

Example 4.3. *(Test of the energy dissipation law) Consider the following Neumann problem:*

$$\begin{cases} \tau\dfrac{\partial\phi}{\partial t} = \varepsilon^2\Delta\phi - \dfrac{1}{2}\phi(\phi^2-1) + \dfrac{2\rho c}{L}u, & \text{in } [-1,1]^2\times(0,T], \\ \dfrac{\partial u}{\partial t} = K\Delta u - \dfrac{L}{2\rho c}\dfrac{\partial\phi}{\partial t}, & \\ \phi(\boldsymbol{x},0) = \phi_0(\boldsymbol{x}), \qquad \forall \boldsymbol{x}\in[-1,1]^2, & \\ u(\boldsymbol{x},0) = u_0(\boldsymbol{x}). & \end{cases} \tag{4.2}$$

We run CN2 scheme with the initial condition

$$\begin{cases} \phi_0(\boldsymbol{x}) = 0.6\sin(\frac{\pi}{2}x)\sin(\frac{\pi}{2}y) + 0.35Rand(x,y), \\ u_0(\boldsymbol{x}) = 0.9\cos(\pi x)\cos(\pi y) + 0.05Rand(x,y), \end{cases}$$

where $Rand(x,y)$ *stands for the random values in* $[-1,1]^2$.

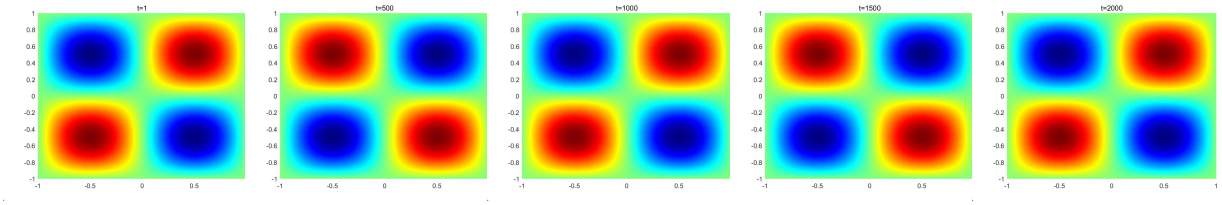

$t = 1$ $t = 500$ $t = 1000$ $t = 1500$ $t = 2000$

(a) computed result of ϕ

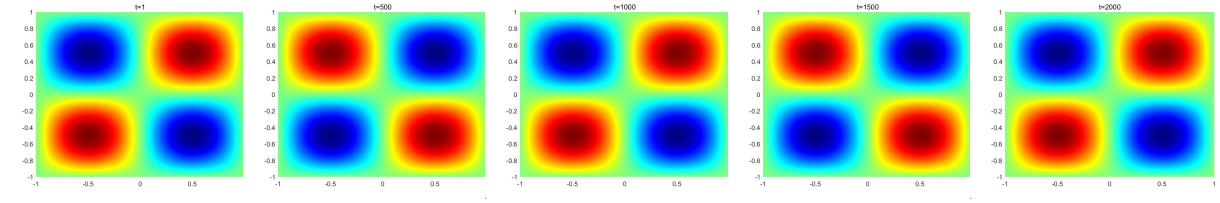

$t = 1$ $t = 500$ $t = 1000$ $t = 1500$ $t = 2000$

(b) exact solution of ϕ

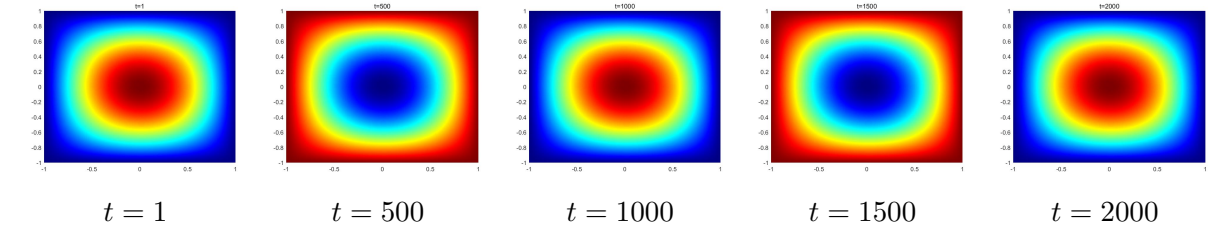

$t = 1$ $t = 500$ $t = 1000$ $t = 1500$ $t = 2000$

(c) computed result of u

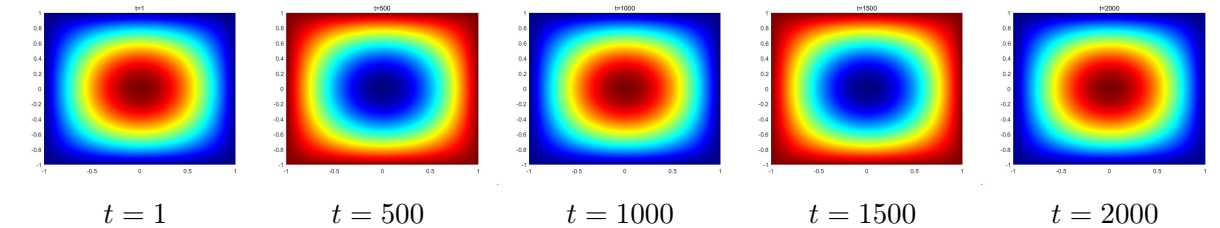

$t = 1$ $t = 500$ $t = 1000$ $t = 1500$ $t = 2000$

(d) exact solution of u

FIGURE 3. (Example 4.1) Comparison between the exact solution and the computed results with $\delta t = 0.5$ at $t = 1, 500, 1000, 1500, 2000$.

In this example, we use the spectral method with $N = 20$ for the spatial approximation. The parameters chosen in this example are: $\tau = \rho = c = L = K = 1$, $\varepsilon^2 = 1e-4$. The main purpose is to compare the original energy and the modified energy. The computed results up to $T = 0.5$ with the time step sizes $\delta t = 0.05, 0.025, 0.01, 0.001, 0.00001$ are plotted in Figure 4. The left figure shows the original energy and the right figure shows the modified energy. We observe: 1) both the original energy and the modified energy are strictly dissipative as expected; 2) the energy curves converge when δt decreases, which is indicative of the convergence of the numerical solution with respect to the time step size.

m	Implicit				Explicit			
	ϕ		u		ϕ		u	
	L_2 error	order	L_2 error	order	L_2 error	order	L_2 error	order
1	1.26E+00	-	1.03E-01	-	1.18E+00	-	1.37E-01	-
2	8.96E-01	0.50	6.05E-02	0.77	9.96E-01	0.25	8.21E-02	0.74
3	5.45E-01	0.72	3.15E-02	0.94	7.13E-01	0.48	4.50E-02	0.87
4	2.88E-01	0.92	1.59E-02	0.99	4.46E-01	0.68	2.36E-02	0.93
5	1.44E-01	1.01	7.91E-03	1.00	2.48E-01	0.85	1.20E-02	0.97
6	7.09E-02	1.02	3.95E-03	1.00	1.28E-01	0.96	6.04E-03	0.99
7	3.51E-02	1.01	1.97E-03	1.00	6.39E-02	1.00	3.02E-03	1.00
8	1.75E-02	1.01	9.85E-04	1.00	3.19E-02	1.00	1.51E-03	1.00
9	8.71E-03	1.00	4.92E-04	1.00	1.59E-02	1.00	7.55E-04	1.00

TABLE 1. (Example 4.2) The L_2 error at $T = 10$ and corresponding orders for the first order scheme with $\delta t = \frac{1}{2^m}$.

m	Implicit				Explicit			
	ϕ		u		ϕ		u	
	L_2 error	order	L_2 error	order	L_2 error	order	L_2 error	order
1	4.93E-01	-	5.45E-02	-	7.03E-01	-	8.80E-02	-
2	7.30E-02	2.75	1.36E-02	2.00	6.14E-01	0.20	3.36E-02	1.39
3	1.60E-02	2.19	3.40E-03	2.00	2.21E-01	1.47	1.35E-02	1.31
4	3.97E-03	2.01	8.42E-04	2.01	5.87E-02	1.91	4.60E-03	1.55
5	9.90E-04	2.00	2.09E-04	2.01	1.48E-02	1.99	1.53E-03	1.59
6	2.47E-04	2.00	6.01E-05	1.80	3.69E-03	2.00	4.43E-04	1.78
7	6.18E-05	2.00	1.74E-05	1.79	9.23E-04	2.00	1.24E-04	1.83
8	1.54E-05	2.00	4.87E-06	1.83	2.31E-04	2.00	3.31E-05	1.91
9	3.86E-06	2.00	1.30E-06	1.91	5.76E-05	2.00	8.62E-06	1.94

TABLE 2. (Example 4.2) The L_2 error at $T = 10$ and corresponding orders for BDF-2 scheme with $\delta t = \frac{1}{2^m}$.

Example 4.4. *(A liquid freezing problem) Consider the thermal phase field model subject to the following boundary condition:*

$$\phi|_{\partial\Omega} = -1, \quad \textit{and} \quad u|_{\partial\Omega} = -0.1,$$

and the initial condition:

$$\begin{cases} \phi(\boldsymbol{x}, 0) = -1, \ u(\boldsymbol{x}, 0) = -0.1, & \forall \boldsymbol{x} \in \partial\Omega, \\ \phi(\boldsymbol{x}, 0) = 1, \quad u(\boldsymbol{x}, 0) = 0, & \textit{else}. \end{cases}$$

The other parameters used in the calculation are: $\tau = 5e-3$, $\varepsilon^2 = 1e-4$, $\rho = c = L = K = 1$. *This computational configuration corresponds to the inward growth of an interface in a square container filled with liquid of the freezing temperature* $u = 0$ *and kept at a constant temperature*

m	Implicit				Explicit			
	ϕ		u		ϕ		u	
	L_2 error	order	L_2 error	order	L_2 error	order	L_2 error	order
1	1.88E-01	-	2.38E-01	-	8.97E-01	-	1.72E-01	-
2	5.61E-02	1.74	1.11E-01	1.10	6.05E-01	0.57	8.10E-02	1.08
3	1.66E-02	1.75	4.11E-02	1.43	2.67E-01	1.18	2.93E-02	1.47
4	4.76E-03	1.81	1.32E-02	1.64	7.80E-02	1.78	9.18E-03	1.68
5	1.33E-03	1.83	3.83E-03	1.79	2.07E-02	1.92	2.61E-03	1.81
6	3.60E-04	1.89	1.04E-03	1.88	5.32E-03	1.96	7.01E-04	1.90
7	9.40E-05	1.94	2.72E-04	1.94	1.35E-03	1.98	1.82E-04	1.95
8	2.40E-05	1.97	6.95E-05	1.97	3.41E-04	1.99	4.63E-05	1.97
9	6.07E-06	1.98	1.76E-05	1.98	8.55E-05	1.99	1.17E-05	1.99

TABLE 3. (Example 4.2) The L_2 error at $T = 10$ and corresponding orders for CN2 scheme with $\delta t = \frac{1}{2^m}$.

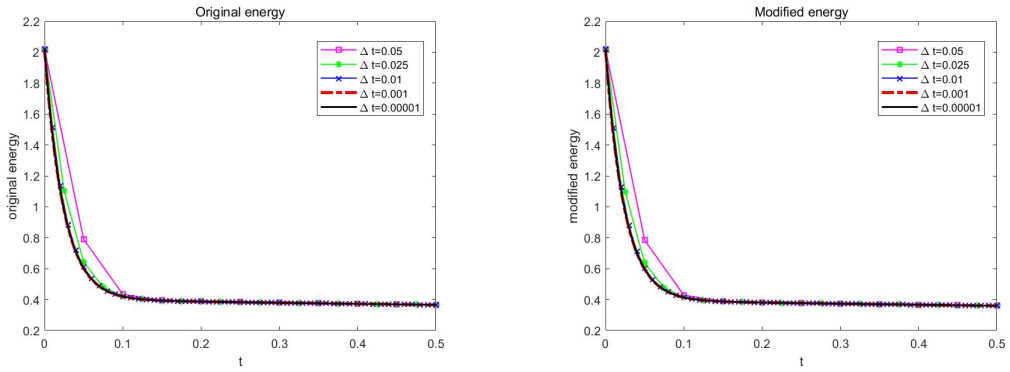

(a) original energy (b) modified energy

FIGURE 4. (Example 4.3) Comparison of the original energy and the modified energy using random initial value. Left: original energy; Right: modified energy.

$u = -0.1$ *at the boundary. This numerical example is similar to the one given in [16], but the computational domain* $\Omega = (-1, 1)^2$ *slightly differs from that in [16].*

The simulation is performed by using BDF-2 scheme (2.22) in time and the Galerkin spectral method with $N = 128$ in space. The simulation results are presented in Figures 5-8. Figure 5 shows how the phase field ϕ and the temperature u evolve over time. Obviously, we can see that the red areas in both phase field and temperature are steadily shrinking as time evolves. In the phase field graphics, boundary between the red area where ϕ is around 1 and the blue area where ϕ is around -1 is clear enough that we can observe how the state change. After a period of time, the phase field will become around -1 with the temperature becoming -0.1 everywhere. To observe the movement of the boundary, we mark the points where the value of ϕ is close to 0 in Figure 6. It shows how the interface between $\phi = -1$ and $\phi = 1$ moves as time progresses until $t = 0.5$. Without tracking the interface, we found those curves after the values of the phase

function are obtained. In order to observe the change process of the phase field and temperature more intuitively, we use Figure 7(a) to show some sample phase field profiles of the middle cross section at different instants and Figure 7(b) gives the corresponding temperature profiles at the corresponding times. It should be noted that the phase jumps across the interface in Figure 7(a) is sharp even though those corresponding temperature in Figure 7(b) has small oscillations. Since the Legendre-Gauss-Lobatto points are not equidistant, Figure 6 cannot directly correspond to Figure 5 and Figure 7(a), but we can still see the change process of the phase field ϕ and the temperature u from these figures. We also plot in Figure 8 the L^2-errors at the final time $T = 0.1$ as functions of the time step size δt in log-log scale. It clearly indicates that the proposed scheme is of second order accuracy for both phase field ϕ and temperature u in this liquid freezing problem. Finally, the results obtained are in agreement with those presented in the reference [16].

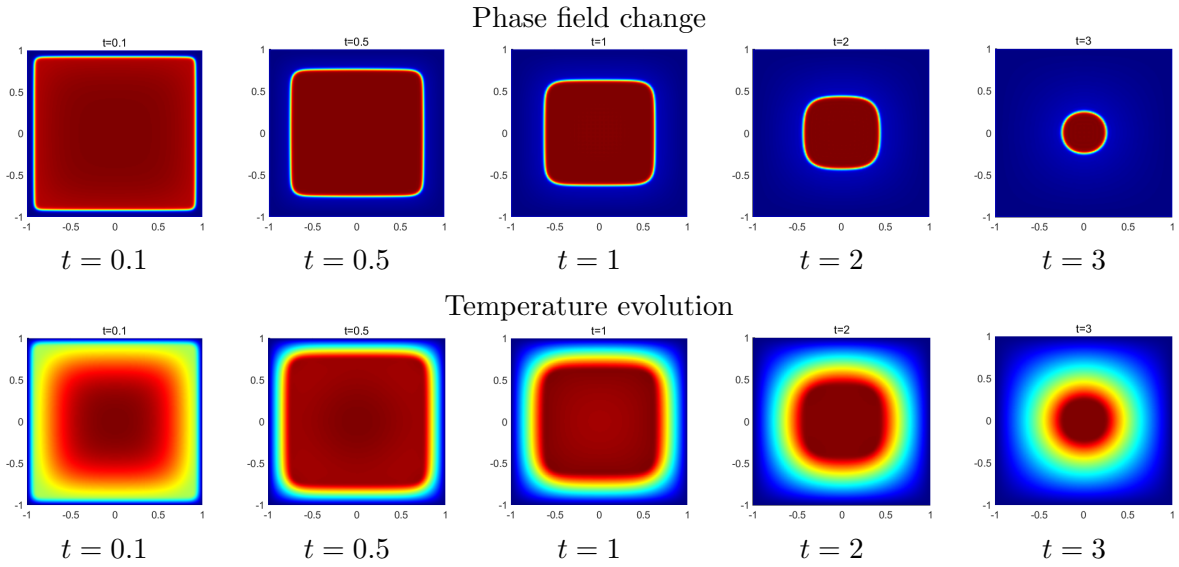

FIGURE 5. (Example 4.4) Results of the phase change simulation. Up: phase field change; Down: temperature evolution.

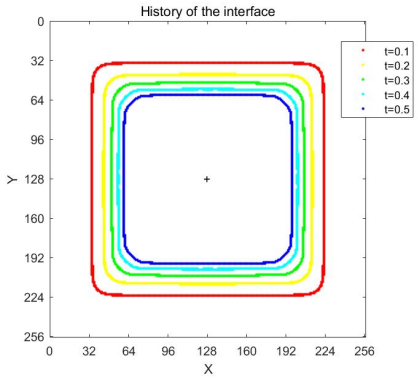

FIGURE 6. (Example 4.4) History of the interface moving towards the center of the domain as time progresses.

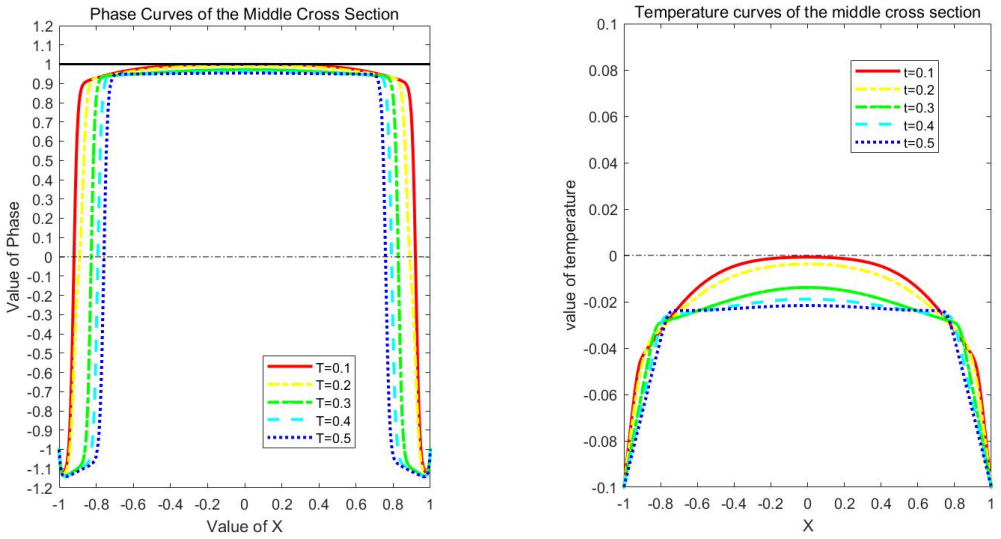

(a) Phase curves. (b) Temperature curves.

FIGURE 7. (Example 4.4) Phase field and temperature profiles of the middle cross section at different instants. Left: phase curves; Right: temperature curves.

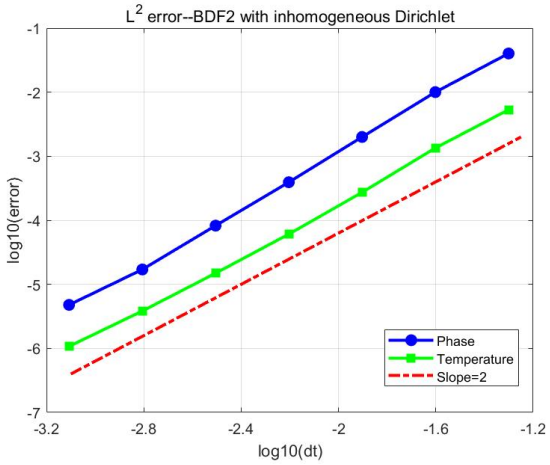

FIGURE 8. (Example 4.4) Error decay at $T = 0.1$ versus the time step sizes for the moving boundary problem.

Example 4.5. *(Simulation with real physical parameters) We propose to end this section by distinguishing the thermal properties of the material in its liquid phase from those in its solid phase. In the previous simulation these parameters were chosen constant to match the data in the reference article and thus to validate our results. In this example we consider a simulation*

for the model having real physical parameters related to the phases of the material:

$$\begin{cases} \tau\dfrac{\partial\phi}{\partial t} = \varepsilon^2\Delta\phi - \dfrac{1}{2}\phi(\phi^2-1) + \dfrac{2\rho(\phi)c(\phi)}{L}u, & \text{in } [-1,1]^2\times(0,T], \\ \dfrac{\partial u}{\partial t} = \nabla\cdot(K(\phi)\nabla u) - \dfrac{L}{2\rho(\phi)c(\phi)}\dfrac{\partial\phi}{\partial t}, \\ \phi(\boldsymbol{x},0) = \phi_0(\boldsymbol{x}), \qquad \forall \boldsymbol{x}\in[-1,1]^2, \\ u(\boldsymbol{x},0) = u_0(\boldsymbol{x}), \end{cases} \tag{4.3}$$

where

$$\begin{cases} \rho = 1470kg/m^3 \\ K = 0.36W/(m\cdot K) \\ c = 1330J/(kg\cdot K) \end{cases} \text{when solid,} \qquad \begin{cases} \rho = 1332kg/m^3 \\ K = 0.52W/(m\cdot K) \\ c = 2360J/(kg\cdot K) \end{cases} \text{when liquid.}$$

The heat Latent coefficient is equal to $L = 267kJ/kg$. For the initial condition, we use the same as in Example 4.4.

Remark 4.1. *The solver developed in this paper is optimal for the case of constant conductivity in the whole domain. The case we consider here presents a small variation that we will approach by imposing it identical and equal to 0.52 $W/(m\cdot K)$. A fast solver for non-constant coefficients is to be developed in the future work.*

The simulation results are shown in Figure 9. It is observed that at $t = 0.05$ most of the area is still in liquid state ($\phi = 1$); at $t = 1.2$, all but the middle part has become solid ($\phi = -1$), which means this material is gradually freezing from liquid to solid over time. This simulation demonstrates the applicability of the proposed method to practical thermal phase change problems.

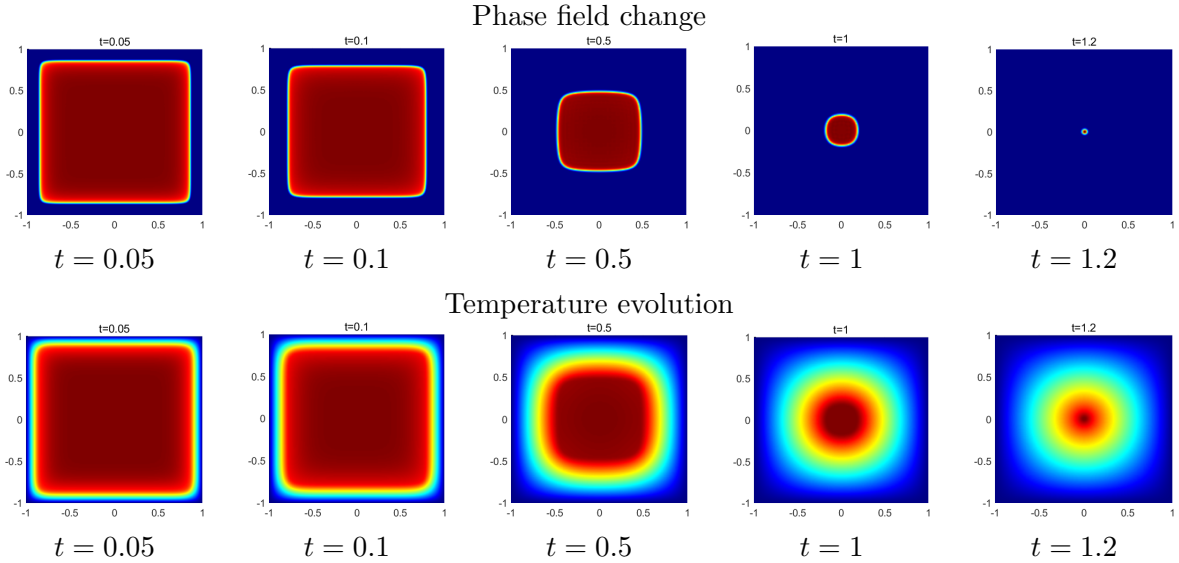

FIGURE 9. (Example 4.5) Results of the phase change simulation. Up: phase field change; Down: temperature evolution.

5. Summary

We have proposed in this paper some new schemes to numerically solve the thermal phase change model, which is a coupling of the Allen-Cahn equation and heat equation. The proposed schemes were constructed based on an auxiliary variable approach to the Allen-Cahn equation and implicit/semi-implicit treatment of the heat equation. The stability property of these schemes was rigorously established, while the temporal/spatial convergence rates were carefully examined through a series of numerical tests. We demonstrated theoretically and numerically that the implicit treatment of the coupling terms leads to unconditionally stable schemes. We also showed that the proposed method is efficient and easy to implement in the sense that only several second-order elliptic problems with constant coefficients need to be solved at each time step. A comparison between the implicit and explicit treatments of the coupling terms was carried out. We emphasize that the explicit schemes are easier to implement, but there is no theoretical guarantee for their unconditional stability, although no instability observed in our calculation. The numerical experiment has shown that the proposed schemes not only achieve the predicted/expected convergence order for the fabricated smooth solutions, but also are capable of simulating correct movement of the solid-liquid boundary of a fluid freezing problem. Finally, the proposed method is expected to be applicable to more complex physical problems, such as dendrite growth models.

References

[1] D. Adalsteinsson and J.A. Sethian. The fast construction of extension velocities in level set methods. *J. Comput. Phys.*, 148:2–22, 1999.

[2] G. Caginalp. An analysis of a phase field model of a free boundary. *Arch. Rational Mech. Anal.*, 92(3):205–245, 1986.

[3] G. Caginalp. Stefan and hele-shaw type models as asymptotic limits of the phase-field equations. *Phys. Rev. A*, 39(11):5887–5896, 1989.

[4] S. Chen, B. Merriman, S. Osher, and P. Smereka. A simple level set method for solving Stefan problems. *J. Comput. Phys.*, 135:8–29, 1997.

[5] Q. Cheng and J. Shen. Multiple scalar auxiliary variable (MSAV) approach and its application to the phase-field vesicle membrane model. *SIAM Journal on Scientific Computing*, 40(6):A3982–A4006, 2018.

[6] J. B. Collins and H. Levine. Diffuse interface model of diffusion-limited crystal growth. *Phys. Rev. B*, 31(9):6119, 1985.

[7] J. Crank. *Free and Moving Boundary Problems*. Clarendon Press, Oxford, 1984.

[8] C. M. Elliott and A.M. Stuart. The global dynamics of discrete semilinear parabolic equations. *SIAM Journal on Numerical Analysis*, 30(6):1622–1663, 1993.

[9] D. J. Eyre. Unconditionally gradient stable time marching the Cahn-Hilliard equation. *Mrs Proceedings*, 529:39–46, 1998.

[10] M. Fabbri and V. R. Voller. The phase-field method in the sharp-interface limit: A comparison between model potentials. *J. Comput. Phys.*, 130(2):256–265, 1997.

[11] G. Fix. Phase field method for free boundary problems. *Free Boundary Problems*, pages 580–589, 1983.

[12] D. Hou, M. Azaiez, and C. Xu. A variant of scalar auxiliary variable approaches for gradient flows. *Journal of Computational Physics*, 395:307–332, 2019.

[13] D. Juric and G. Tryggvason. A front-tracking method for dendritic solidification. *J. Comput. Phys.*, 123:127–148, 1996.

[14] Y.C. Lam, J.C. Chai, P. Rath, H. Zheng, and V.M. Murukeshan. A fixed-grid method for chemical etching. *Int. Commun. Heat Mass Transfer*, 31:1123–1131, 2004.

[15] J. S. Langer. Models of pattern formation in first-order phase transitions. *Directions in Condensed Matter Physics*, pages 164–186, 1986.

[16] J. T. Lin. The numerical analysis of a phase field model in moving boundary problems. *SIAM Journal on Numerical Analysis*, 25(5):1015–1031, 1988.

[17] J. A. Mackenzie and M. L. Robertson. A moving mesh method for the solution of the one-dimensional phase-field equations. *J. Comput. Phys.*, 181(2):526–544, 2002.

[18] W.J. Minkowycz and E.M. Sparrow. *Advances in Numerical Heat Transfer*, volume 1. Taylor & Francis, Washington, 1997.

[19] W.D. Murray and F. Landis. Numerical and machine solutions of transient heat-conduction problems involving melting or freezing. *Trans. ASME (C) J. Heat Transfer*, 81:106–112, 1959.

[20] S. Osher and R. Fedkiw. *Level Set Methods and Dynamic Implicit Surfaces*. Springer, New York, 2003.

[21] S. Osher and J.A. Sethian. Fronts propagating with curvature-dependent speed: algorithms based on Hamilton-Jacobi formulations. *J. Comput. Phys.*, 79:12–49, 1988.

[22] L. I. Rubinstein. *The Stefan Problem*. American Mathematical Society, Providence, 1971.

[23] A. Schmidt. Computation of three dimensional dendrites with finite elements. *J. Comput. Phys.*, 125:293–312, 1996.

[24] G. Segal, C. Vuik, and F. Vermolen. A conserving discretization for the free boundary in a two-dimensional Stefan problem. *J. Comput. Phys.*, 141:1–21, 1998.

[25] J.A. Sethian. *Level Set Methods and Fast Marching Methods*. Cambridge University Press, New York, 1999.

[26] J. Shen, T. Tang, and L. Wang. *Spectral methods : algorithms, analysis and applications*. Springer, Berlin, 2010.

[27] J. Shen, J. Xu, and J. Yang. The scalar auxiliary variable (SAV) approach for gradient flows. *J. Comput. Phys.*, 353:407–416, 2018.

[28] J. Shen, J. Xu, and J. Yang. A new class of efficient and robust energy stable schemes for gradient flows. *SIAM Rev.*, 61(3):474–506, 2020.

[29] J. Shen and X. Yang. Numerical approximations of Allen-Cahn and Cahn-Hilliard equations. *Discrete Contin. Dyn. Syst.*, 28:1669–1691, 2010.

[30] J. Stefan. Ueber die theorie der eisbildung, insbesondere ber die eisbildung im polarmeere. *Annalen der Physik*, 1891.

[31] M. Sussman, P. Smereka, and S. Osher. A level set approach for computing solutions to incompressible two-phase flow. *J. Comput. Phys.*, 114:146–159, 1994.

[32] A. A. Wheeler, W. J. Boettinger, and G. B. Mcfadden. Phase-field model for isothermal phase transitions in binary alloys. *Phys.Rev. A*, 45(10):7424–7439, 1992.

[33] X. Yang. Linear, first and second-order, unconditionally energy stable numerical schemes for the phase field model of homopolymer blends. *J. Comput. Phys.*, 327:294–316, 2016.

[34] X. Yang, J. Zhao, Q. Wang, and J. Shen. Numerical approximations for a three components Cahn-Hilliard phase-field model based on the invariant energy quadratization method. *Math.*

Models Methods Appl. Sci., 327(11), 2017.

[35] P. Yue, J. Feng, C. Liu, and J. Shen. A diffuse-interface method for simulating two-phase flows of complex fluids. *Journal of Fluid Mechanics*, 515(1):293–317, 2004.

[36] J. Zhang, C. Chen, and X. Yang. A novel decoupled and stable scheme for an anisotropic phase-field dendritic crystal growth model. *Applied Mathematics Letters*, 95:122–129, 2019.

[37] J. Zhang and X. Yang. A fully decoupled, linear and unconditionally energy stable numerical scheme for a melt-convective phase-field dendritic solidification model. *Computer Methods in Applied Mechanics and Engineering*, 363, 2020.

[38] J. Zhao, Q. Wang, and X. Yang. Numerical approximations for a phase field dendritic crystal growth model based on the invariant energy quadratization approach. *Int. J. Numer. Meth. Eng.*, 110(3):279–300, 2016.

[39] J. Zhao, X. Yang, Y. Gong, and Q. Wang. A novel linear second order unconditionally energy stable scheme for a hydrodynamic Q-tensor model of liquid crystals. *Comput. Methods Appl. Mech. Eng.*, 318:803–825, 2017.

[40] J. Zhu, L. Chen, J. Shen, and V. Tikare. Coarsening kinetics from a variable-mobility Cahn-Hilliard equation: Application of a semi-implicit fourier spectral method. *Phys. Rev. E*, 60(4):3564–3572, 1999.